ANNUAL REVIEWS

Annual Review of Astronomy and Astrophysics

Protoplanetary Disk Chemistry

Karin I. Öberg,[1] Stefano Facchini,[2] and Dana E. Anderson[3]

[1]Center for Astrophysics, Harvard–Smithsonian, Cambridge, Massachusetts, USA; email: koberg@cfa.harvard.edu

[2]Dipartimento di Fisica, Università degli Studi di Milano, Milano, Italy

[3]Earth and Planets Laboratory, Carnegie Institution for Science, Washington, DC, USA

Annu. Rev. Astron. Astrophys. 2023. 61:287–328

First published as a Review in Advance on June 7, 2023

The *Annual Review of Astronomy and Astrophysics* is online at astro.annualreviews.org

https://doi.org/10.1146/annurev-astro-022823-040820

Keywords

astrochemistry, planet formation, protoplanetary disks

Abstract

Planets form in disks of gas and dust around young stars. The disk molecular reservoirs and their chemical evolution affect all aspects of planet formation, from the coagulation of dust grains into pebbles to the elemental and molecular compositions of the mature planet. Disk chemistry also enables unique probes of disk structures and dynamics, including those directly linked to ongoing planet formation. We review the protoplanetary disk chemistry of the volatile elements H, O, C, N, S, and P; the associated observational and theoretical methods; and the links between disk and planet chemical compositions. Three takeaways from this review are:

- The disk chemical composition, including the organic reservoirs, is set by both inheritance and in situ chemistry.
- Disk gas and solid O/C/N/H elemental ratios often deviate from stellar values due to a combination of condensation of molecular carriers, chemistry, and dynamics.
- Chemical, physical, and dynamical processes in disks are closely linked, which complicates disk chemistry modeling, but these links also present an opportunity to develop chemical probes of different aspects of disk evolution and planet formation.

Contents

1. INTRODUCTION

1.1. Motivation and Scope of Review

Protoplanetary disks are planet-forming, potentially planet-containing, dust- and gas-rich disks around young stars. Disk chemical compositions determine the elemental and molecular makeup of forming planets and influence many other disk properties relevant to planet formation. Disk chemistry also provides some of our best tools to characterize disk structures and dynamics, including the presence of protoplanets. Developing a predictive theory of planet formation therefore requires a deep understanding of the chemistry of protoplanetary disks. This is true for all kinds of planets but is perhaps especially salient when considering how often temperate planets in our Galaxy may be chemically hospitable to life (i.e., have access to water and a suitable combination of organic and inorganic material).

The aims of this review are to introduce the study of disk chemistry; to present our current state of knowledge emerging from the past two decades of observational, theoretical, and experimental research; and to propose some possible paths forward. We limit the scope of the review in two important aspects. First, we treat only protoplanetary disks (i.e., circumstellar disks around 1–10 Myr old stars), around which the natal envelope has been cleared; therefore, we do

not include the chemistry of younger protostellar disks or the debris disks found around older stars. Second, we focus on the volatile elements and molecules and therefore largely ignore the physics and chemistry of refractory elements bound up in dust particles. For the purpose of this review, a volatile element or molecule is any species that is present as a liquid or gas under typical terrestrial conditions, which includes most small and midsized hydrogen (H), oxygen (O), carbon (C), nitrogen (N), sulfur (S), and phosphorus (P) molecules. The scope of this review, then, is the distributions and chemistry of volatiles in protoplanetary disks.

1.2. Context: Protoplanetary Disk Formation and Evolution

Protoplanetary disks emerge within the context of star formation, when infalling interstellar cloud material becomes distributed in disk-like structures to preserve angular momentum (Shu et al. 1987). The chemical composition of the resulting disk likely depends on both disk chemical processes and chemical inheritance from the preceding interstellar and protostellar phases (e.g., Visser et al. 2009). The links between interstellar, protostellar, and disk compositions were recently reviewed by Öberg & Bergin (2021), Bergin et al. (2023), and van Dishoeck & Bergin (2021), and protostellar organic chemistry by Jørgensen et al. (2020). Here, we simply summarize a few aspects of interstellar and protostellar chemistry that are especially relevant for protoplanetary disks and planet formation.

In the diffuse interstellar medium (ISM), a substantial fraction of O and half of the C are incorporated into refractory grains. The remaining C and O, as well as most N and H, become bound up in stable molecules such as H_2, CO, CO_2, N_2, NH_3, and H_2O at the interstellar cloud stage. Many of these carriers survive disk formation. Their chemical reactivities (or lack thereof) and different volatilities affect the distribution of major volatile elements in disks. Molecular clouds also produce the first generation of organic molecules, including carbon chains, CH_4, CH_3OH, and more complex organics. At the onset of star and planet formation in molecular clouds, most of these molecules are found in icy grain mantles. In the subsequent protostellar phase, additional complex organics form. These interstellar volatiles and simple and complex organics can all become incorporated into disks, setting the initial conditions for disk chemistry.

The second context for this review is the local environment within which a disk is situated—the environment surrounding the disk sets the external radiation field, and may dynamically shape the disk structure and continue to feed the disk with gas and dust (Walsh et al. 2014, Andrews 2015, Huang et al. 2021)—as well as the disk's evolving structure and dynamical processes (**Figure 1**). Protoplanetary disks were recently reviewed by Andrews (2020), while Aikawa et al. (2022) provide an introduction to many disk structures and processes relevant for disk chemistry.

The disk surface density is set by a combination of infall of material from the natal cloud and protostellar envelope, inward gas accretion, outward gas spreading, accretion onto the star, disk winds, ongoing planet formation, and other gap-opening mechanisms (e.g., Lynden-Bell & Pringle 1974, Bai & Stone 2013, Andrews et al. 2018). Within disks, gas and dust are transported both vertically and radially. Vertical gas transport happens through large-scale turbulence, diffusion, and meridional flows into disk gaps (e.g., Meijerink et al. 2009, Semenov & Wiebe 2011, Teague et al. 2019), while solids are preferentially moved toward the midplane as a result of grain growth and settling. Radially, gas and small entrained grains are transported through advection, turbulent diffusion, and disk winds, while larger dust grains partially decouple from the gas and drift toward pressure maxima, which in the absence of substructure entails inward transport of solids (e.g., Ciesla & Cuzzi 2006, D'Alessio et al. 2006). Therefore, we should expect transport of gas and solids both between the outer low-density and inner high-density disk regions and between the disk midplane and elevated layers.

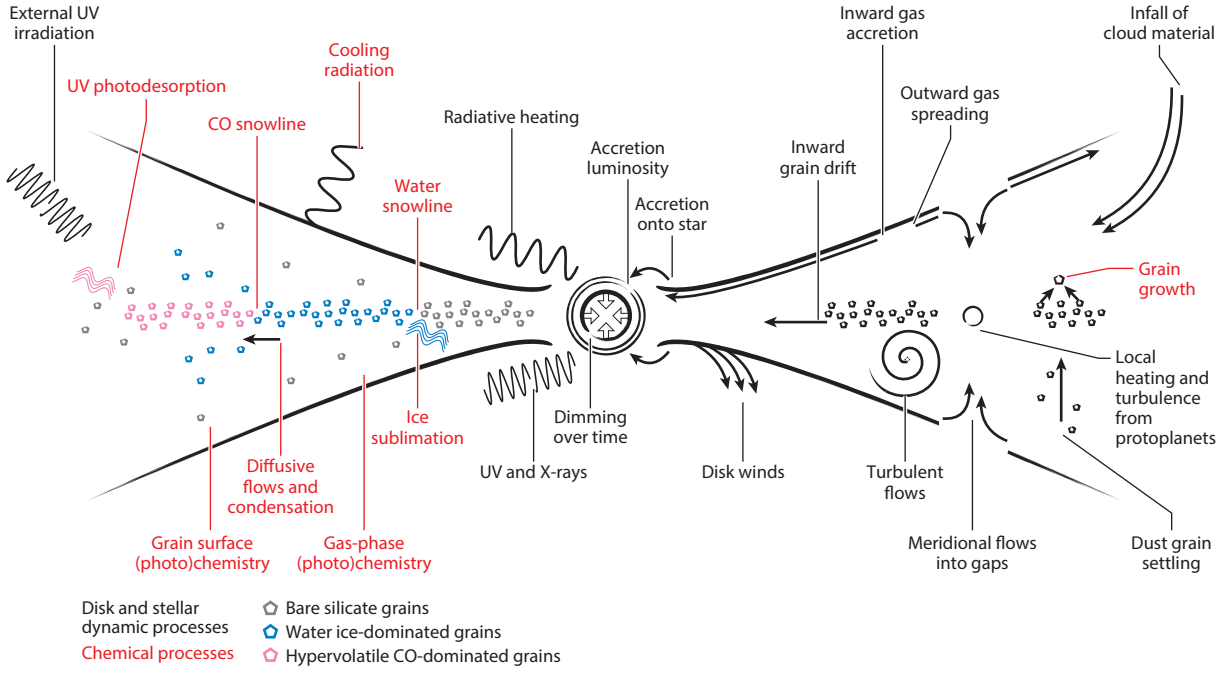

Figure 1

A nonexhaustive overview of the many processes in disks that directly influence the chemistry and the distribution of molecules, depend on the disk molecular composition, are traced by molecular lines, and/or directly involve the destruction or formation of molecules or molecular phases. The processes labeled in black are stellar and disk dynamical processes that act on disk gas and dust regardless of their particular chemical makeup. Processes labeled in red are either chemical processes or processes that depend directly on the chemical composition. On the left, bare silicate grains are shown in gray; water ice–dominated grains in blue; and grains with a large reservoir of hypervolatiles, including CO, in pink.

Disks are heated by stellar radiation, radiation from accretion shocks onto the star, and viscous dissipation (e.g., D'Alessio et al. 1999), all of which decrease over time as a result of stellar contraction and a decreasing accretion rate. The decrease is not monotonic, however, and luminosity bursts may temporarily change the disk temperature structure (e.g., Armitage et al. 2001). The disk temperature further depends on the distribution of solids and molecules in the disk atmosphere, which control cooling and heating in the disk (Woitke et al. 2009). At disk radii dominated by radiative heating, the disk temperature increases with disk height. Disks are also irradiated by UV, X-rays, and cosmic rays from both the central star and external sources (e.g., Kastner et al. 1997, Cleeves et al. 2015b, Rab et al. 2018). The radiative transport of these high-energy particles and radiation is complex, especially in the presence of dust evolution and substructure, but generally the fluxes are high in the disk atmosphere and increasingly depleted toward the disk midplane.

1.3. An Introduction to Inner and Outer Disk Chemistry

When surveying the chemical processes that govern the distributions and evolution of volatiles in disks, it is useful to consider the disk region interior to the water condensation front or snowline (the inner disk where terrestrial planets form) separately from the rest of the disk (the outer disk where gas and ice giants as well as comets originate). Depending on the stellar luminosity, this boundary between inner and outer disk falls between a fraction of an astronomical unit and ~10 au. In the inner disk, high densities and temperatures result in complete sublimation of

volatiles and short chemical timescales in the gas phase that reset the chemistry (e.g., Glassgold et al. 2009, Pontoppidan et al. 2014, and references therein). In contrast to most phases of star and planet formation, three-body reactions, endothermic reactions, and reactions with substantial energy barriers may all be possible. The inner disk may be considered to have an inner boundary at the silicate condensation line (Kress et al. 2010), and in between this and the water snowline, it should host a soot line, where large C molecules and small C grains volatilize. Despite its high densities and temperatures, the inner disk chemistry may not be at equilibrium because of strong irradiation fields impinging on the disk atmosphere (e.g., Ádámkovics et al. 2014) and continuous transport of material from the outer disk.

Outer disk chemistry has been reviewed by Henning & Semenov (2013), Dutrey et al. (2014), and Aikawa et al. (2022). In the outer disk, inheritance cannot be ignored, especially in the disk midplane, where interstellar and protostellar chemical products may be preserved (Visser et al. 2009). As a result, the outer disk likely begins with much of its O tied up in H_2O- and CO_2-rich ices and therefore taken out of circulation from the gas phase. Outer disks are chemically stratified both radially and vertically due to 2D condensation fronts, which are referred to as snowlines in the disk midplane, and the dependence of chemical reactions on density, temperature, ionization, and dissociative radiation (Aikawa et al. 2002). The disk midplane may be chemically inert, simply preserving inherited reservoirs, or quite chemically active, depending on its access to ionizing irradiation (Cleeves et al. 2015b). In somewhat elevated disk layers, neutral–neutral and ion–molecule gas-phase reactions operate together with grain surface chemistry to produce a so-called molecular layer, where the chemistry is neither completely reset nor completely inherited. Finally, the outer disk atmosphere is characterized by relatively low densities, moderately high temperatures, and high irradiation fields, which drive a rapid radical- and ion-based chemistry that is qualitatively similar to that of a classical photon-dominated region (PDR). These different layers may all be dynamically and therefore chemically connected, however, blurring some of the described differences.

2. DISK CHEMISTRY MODELING

Disk chemistry models are used to provide interpretative frameworks for observations, to expand the kinds of species that can be characterized in disks beyond what is directly observable, and to connect different evolutionary phases up until and sometimes including planet formation. In this section, we introduce astrochemical modeling, starting with how to set up the "physical" disk structure (Section 2.1), followed by different treatments of chemistry within such a framework (Section 2.2) and interactions between chemistry and dynamics (Section 2.3).

2.1. Establishing the Disk Physical Structure

Chemical reactivity depends on the local gas and dust grain densities, dust grain optical and material properties, gas and dust grain temperatures, energetic radiation fields, and ionization rates. Establishing these can be done relatively self-consistently by taking into account the interdependence of gas and dust densities and temperatures, radiation fields, and chemistry, but parametric structures are also frequently used to simplify the modeling process, or some aspect of it. The choice of approach depends ultimately on the scientific question at hand, and especially on the acceptable computational expense of each model run. **Figure 2** illustrates some common approaches that are described below.

The establishment of the disk physical parameters begins with choosing an initial gas and dust density 2D structure using, for example, the steady-state solution for a protoplanetary disk undergoing viscous evolution (Lynden-Bell & Pringle 1974, Hartmann et al. 1998) or parameterizations

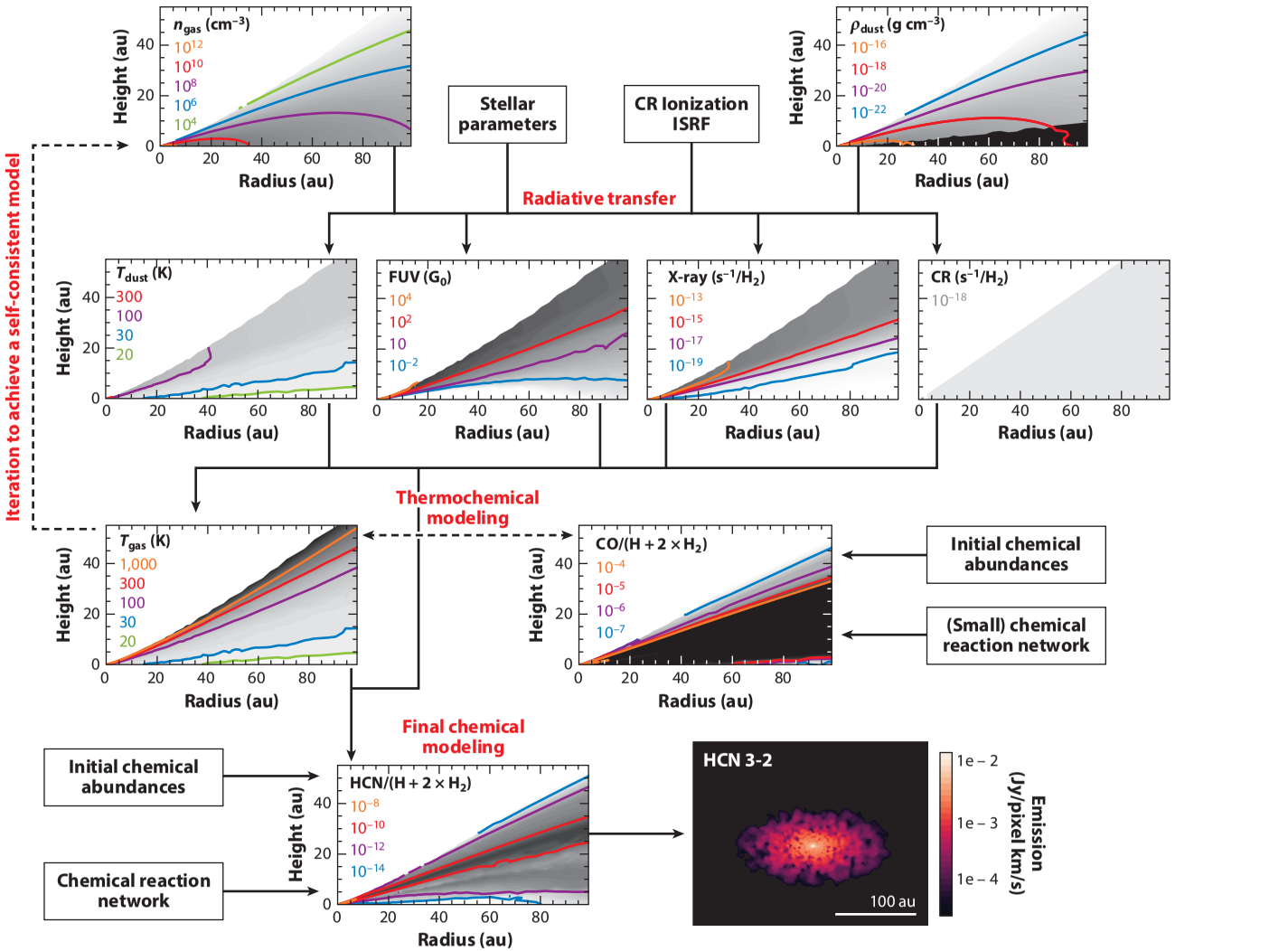

(*Caption appears on following page*)

Figure 2 (*Figure appears on preceding page*)

The steps involved in a typical disk chemistry modeling framework. (*Top to bottom*) (Initial) gas and dust density structures are combined with stellar parameters and the local irradiation environment to calculate the disk temperature, radiation, and ionization structures using radiative transfer. If a self-consistent model is desired, these are then updated iteratively, taking into account the effect of chemical abundances on cooling and heating in a thermochemical modeling step. The final chemical abundances are determined once the disk physical structure has converged, and the observable molecular line properties are calculated using radiative transfer. Abbreviations: CR, cosmic ray; FUV, far ultraviolet; ISRF, interstellar radiation field.

based on the minimum-mass Solar Nebula or on observations of disks (e.g., Chiang & Youdin 2010, K. Zhang et al. 2021). The vertical density distribution depends on the disk temperature, which can be accounted for by iteratively computing the gas temperature and vertical density distribution (e.g., Nomura et al. 2007, Woitke et al. 2009, Bruderer et al. 2012). The dust density structure commonly involves one or two dust populations, each described by a grain size distribution, set of opacities, and radial and vertical distribution; small dust grains (up to micrometer sizes) are assumed to couple to the gas, while larger grains are not (e.g., D'Alessio et al. 2006). The precise choice of dust properties can have a big impact on the model because dust affects ionization, heating, cooling, and chemistry (e.g., Gavino et al. 2021). While smoothly varying disks have been the norm in models, (sub)millimeter observations have motivated the investigation of more complex cases like transition disks and disks with gaps opened by forming planets (e.g., Facchini et al. 2018b, Alarcón et al. 2020).

The disk gas and dust temperature, UV and X-ray radiation fields, and ionization fractions can be initially estimated through radiative transfer calculations using the abovementioned density structures (e.g., van Zadelhoff et al. 2003, Nomura et al. 2007, Bethell & Bergin 2011, Rab et al. 2018) (**Figure 2**). The temperature calculations also need to take into account viscous heating in the dense inner disk midplane and the decoupling of gas and dust temperatures in the disk atmosphere (Glassgold et al. 2004). The latter effect can be solved explicitly by taking into account dust and gas heating and cooling processes (Kamp & Dullemond 2004). These processes depend on the gas chemical composition; therefore, self-consistent determination of the temperature structure can only be done using thermochemical models that iteratively calculate the disk gas temperature and chemical abundances (Woitke et al. 2009, Bruderer et al. 2012, Du & Bergin 2014). Finally, cosmic rays permeate through the entire disk and are typically incorporated at or below the H ionization rate in dense interstellar clouds (e.g., Cleeves et al. 2015b). Additional sources of ionization include radioactive decay and stellar energetic particles (Cleeves et al. 2014, Rab et al. 2017).

All of the above disk characteristics can also be approximated parametrically. The dust and gas density structures can be calculated by first adopting a surface density profile and a radial temperature profile and then calculating vertical densities by assuming hydrostatic equilibrium (Chiang & Goldreich 1997) or prescribing a Gaussian profile with a scale height (e.g., Bruderer 2013). The vertical temperature structure is frequently estimated using the prescription of Dartois et al. (2003). Gas and dust thermal decoupling can also be approximated with a parametric function (Pinte et al. 2006, Cleeves et al. 2015b). The energetic radiation fields and ionization rates can be parameterized as a function of H column density and a chosen dust-to-gas ratio (e.g., Wakelam et al. 2016, Le Gal et al. 2019b). In practice, most models combine parametric elements with self-consistent calculations that take into account some aspects of the interdependencies between chemistry, temperatures, dust and gas vertical density structures, and/or UV and X-ray radiation.

2.2. Treatments of Chemistry

Early theoretical research on chemistry in protoplanetary disks relied largely on thermochemical equilibrium calculations (see Prinn 1993). While potentially appropriate for the inner disk

midplane, inner disk atmospheres and all layers in the outer disk require a nonequilibrium treatment. Building on interstellar chemistry codes (van Dishoeck et al. 1993, Bergin et al. 1995), Aikawa et al. (1996) developed one of the first time-dependent, rate equation–based disk chemistry models where abundances are calculated numerically on the basis of formation and destruction rates, which depend on rate coefficients and abundances supplied from the previous time step. This kind of model then requires initial chemical abundances and an appropriate reaction network, in addition to pre- or cocalculated disk density, temperature, and radiation structures (**Figure 2**).

There are two common choices of initial disk chemical abundances: inheritance of protostellar abundances, where the abundances are supplied by interstellar or protostellar observations or models (e.g., Nomura et al. 2009, Walsh et al. 2015), and "reset" compositions that use high-temperature thermal equilibrium products (Aikawa & Herbst 1999) or assume a fully atomic composition (except for H_2) (e.g., Walsh et al. 2010, Ballering et al. 2021). Based on chemical timescales, the reset approach is a reasonable approximation for models that focus on the chemistry of the inner disk or disk atmosphere, while molecular inheritance becomes increasingly important toward the cold and dense outer midplane (Visser et al. 2009, Drozdovskaya et al. 2016, Eistrup et al. 2016). An additional aspect of the initial conditions concerns the elemental abundance ratios, which are often assumed to be nonsolar (e.g., Najita et al. 2011, Cleeves et al. 2018) on the basis of observational evidence (e.g., Du et al. 2015, Miotello et al. 2019).

The complexity of the model chemical reaction kinetic rate network can range from considering only phase changes of major volatile species (e.g., Piso et al. 2015) to incorporating large and comprehensive kinetic rate networks of chemical reactions (Henning & Semenov 2013 and references therein). The simpler chemical models have been used to establish qualitative interpretative frameworks and to couple disk dynamics and time-dependent chemistry. "Full" chemical reaction networks always include various forms of two-body chemical reactions; UV-, X-ray-, and cosmic-ray-driven chemistry; adsorption and desorption of gas molecules on grain surfaces; and simple surface chemistry, such as the formation of H_2 (e.g., McElroy et al. 2013). Reaction data are available in databases like the UMIST Database for Astrochemistry (McElroy et al. 2013) and KIDA (Wakelam et al. 2012), from which appropriate chemical reaction networks can be developed (e.g., Semenov et al. 2004, Kamp et al. 2017). Additional reactions are then added, depending on the particular science question. Models developed to treat the formation of organic molecules and/or the chemical evolution of icy grain mantles add surface chemistry reactions (Walsh et al. 2015, Ruaud & Gorti 2019, Furuya et al. 2022), often inspired by protostellar chemistry models (Jørgensen et al. 2020 and references therein). Models focused on the inner disk often expand their networks to include high-temperature gas-phase chemistry, three-body reactions, and/or warm surface chemistry (Agúndez et al. 2008, Thi et al. 2020, Anderson et al. 2021). Isotope fractionation is included in models where the precise distributions of minor isotopologues are important (e.g., Aikawa & Herbst 1999, Lyons & Young 2005, Willacy & Woods 2009, Miotello et al. 2014, Visser et al. 2018). To compare the calculated chemical structures (densities and column densities) with observations, one can input the disk gas and dust density and temperature structures, the chemical abundance of the emitting species, and molecular line excitation data into a radiative transfer code (e.g., Brinch & Hogerheijde 2010) and then an observational simulator (the final step in **Figure 2**).

2.3. Modeling Chemistry in a Dynamical Disk Environment

There is a growing list of observations that are difficult to explain with static models, and a frontier in disk chemistry modeling is the comodeling of chemistry and dynamical processes that occur on timescales similar to those of chemical reactions. Simulating the combined effects of all major physical, chemical, and dynamical processes throughout the entire disk is currently too

computationally expensive, however, and models therefore need to choose which physical and chemical processes to include and exclude. Several models incorporate aspects of vertical mixing (e.g., Semenov & Wiebe 2011, Furuya & Aikawa 2014), radial gas diffusion (e.g., Aikawa & Herbst 1999, Ilgner et al. 2004, Nomura et al. 2009, Bosman et al. 2018, Price et al. 2020), and dust evolution (e.g., Vasyunin et al. 2011, Akimkin et al. 2013, Krijt et al. 2018, Booth & Ilee 2019, Eistrup & Henning 2022, Van Clepper et al. 2022), but many of them consider a simplified chemistry (i.e., they are not necessarily more complete than static models with larger chemical networks).

In addition to local mass transport processes, some models consider how global environmental changes affect the chemistry. The effects of stellar evolution have been explored by solving for chemical abundances while altering the disk environment at specified time steps (Price et al. 2020). The impact of short-lived accretion outbursts from the young star on disk compositions has also been investigated (Cleeves et al. 2017, Rab et al. 2017). The outbursts generate chemical changes that persist beyond the duration of the event (Molyarova et al. 2018), but the potential for long-term chemical changes or alteration of planetary compositions by such phenomena has yet to be determined.

3. DISK CHEMISTRY OBSERVATIONS

Disk chemistry is observationally characterized through a range of techniques, which we review in Section 3.1. These observations directly produce molecular line emission fluxes or absorption depths, from which molecular column densities, abundance structures, or higher-level constraints on the disk chemistry and its environment can be retrieved (Section 3.2). In Section 3.3 we present the molecules detected to date, and in Section 3.4 we provide an overview of how molecular inventories, column densities, and abundances vary between disks. Finally, in Sections 3.5 and 3.6 we review observations of radial and vertical structures in disks.

3.1. Observational Techniques

An observational chemical characterization of protoplanetary disks can be achieved by spectroscopic studies at a wide range of frequencies and energy scales probing electronic, vibrational, and rotational transitions of atoms, molecules, and ions. Each wavelength and technique probes a unique aspect of the disk chemistry, and a comprehensive disk chemical characterization requires observations across the electromagnetic spectrum.

Starting at the high-energy end of the spectrum, X-ray and UV transitions are used to probe the elemental abundances of gas and dust that are being accreted onto the stellar surface, providing access to the composition of inner disk refractories (e.g., Drake et al. 2005, Ardila et al. 2013, Kama et al. 2016, Günther et al. 2018). UV observations of fluorescent H_2 and CO transitions are also used to probe hot gas in the innermost disk region, including its C/O/H ratio (France et al. 2012, Arulanantham et al. 2021). Optical spectroscopy can be used to constrain the elemental composition of the innermost disk regions (e.g., Facchini et al. 2016) and to characterize the compositions and dynamics of disk winds from the upper layers of the inner disk regions (Pascucci et al. 2022 and references therein).

The near- to mid-infrared (NIR–MIR) regime enables observations of rovibrational and highly excited rotational lines of simple molecules in the upper layers of the inner few astronomical units of disks, where temperatures and densities are high enough to collisionally excite these transitions (Pontoppidan et al. 2014 and references therein). From space, the *Spitzer* mission was instrumental in surveying numerous disks in MIR emission lines (e.g., Carr & Najita 2008, Salyk et al. 2011b), but at fairly low spectral resolution ($\lambda/\Delta\lambda < 700$). These observations have been complemented with high-resolution spectroscopy from the ground, which avoids line blending and enables

spectrotomographic characterizations of the radial origin of the emission lines (e.g., Brittain et al. 2007, Pontoppidan et al. 2010, Najita et al. 2018, Salyk et al. 2019, Banzatti et al. 2022). Line absorption observations are possible in disks with favorable inclinations and are used to provide complementary constraints on the gas inventory (e.g., Gibb et al. 2007, Najita et al. 2021). The NIR–MIR regime also enables observations of polycyclic aromatic hydrocarbons (PAHs) (Tielens 2008 and references therein) and disk solid-state features, including ice compositions, through (*a*) absorption spectroscopy against an IR bright source, usually performed on edge-on disks (Thi et al. 2002, Pontoppidan et al. 2005, Aikawa et al. 2012, Terada & Tokunaga 2017), and (*b*) scattered light observations of water ice across the 3 μm range (Honda et al. 2009). Observations at these wavelengths are set to be transformed by the *James Webb Space Telescope* (JWST).

In the far infrared (FIR), most spectroscopic surveys have been performed with the *Herschel* mission because of the prohibitive atmospheric transmission at these wavelengths. FIR wavelengths provide access to ground-state transitions of small hydrides, including HD and H_2O (Bergin et al. 2013, Salinas et al. 2016, van Dishoeck et al. 2021); [OI], [CI], and [CII]; and highly excited CO rotational transitions (Bruderer et al. 2012, Meeus et al. 2013, van der Wiel et al. 2014, Fedele et al. 2016). The FIR can also be used to probe water ice thermal emission features (van den Ancker et al. 2000, Min et al. 2016).

Finally, submillimeter and millimeter observations enable the spectroscopic characterization of cold gas, which includes most of the disk gas reservoir. Many small and abundant molecules present rotational transitions at these wavelengths, with typical upper energy levels of 5–500 K. Depending on line and dust optical depths, these observations can probe all the way to the disk midplane, but more often access the outer disk upper layers. Millimeter lines were originally surveyed in disks using single-dish telescopes (Dutrey et al. 1996; Thi et al. 2004; Guilloteau et al. 2013, 2016). The development of (sub)millimeter interferometers enabled the first spatially resolved disk chemistry studies at high spectral resolution ($\lambda/\Delta\lambda < 10^7$) (e.g., Sargent & Beckwith 1987, Qi et al. 2003, Dutrey et al. 2007). In 2011–2014, (sub)millimeter observations of disks were transformed by the arrival of the Atacama Large Millimeter and Submillimeter Array (ALMA), whose collecting area and long baselines enable the detection of rarer molecules and the study of disk chemistry at higher spatial resolution down to scales of 10 au (Öberg et al. 2015b, Huang et al. 2018a). So far, disk chemistry has not been accessible at longer wavelengths, but in the future a more sensitive radio array may provide access to NH_3 and large organic molecules in the disk midplane.

3.2. Retrieval of Molecular Column Densities and Abundances

Molecular line emission strengths depend on molecular column densities and excitation, and on whether both are homogeneous within the beam. Deriving molecular column densities, abundances, and/or information about the disk structure from molecular line observations is therefore not trivial, and full forward modeling (**Figure 2**) is the only way to fully account for these complexities when retrieving disk chemical properties. Forward modeling has been used to derive disk chemical properties of individual sources using highly tuned models (e.g., Cleeves et al. 2018, Calahan et al. 2021a), as well as the generation of large grids of models that can then be compared with observed disks with a range of properties (Miotello et al. 2016, Woitke et al. 2019). For many applications, however, the computational cost of full forward modeling is prohibitive [but see recent initiatives to reduce computational cost using machine learning (Smirnov-Pinchukov et al. 2022)] or impractical due to poor constraints on the disk structure. In these cases, useful retrievals can still be made under some simplifying assumptions.

The simplest retrievals assume that the molecule excitation is well described by local thermodynamic equilibrium (LTE), optically thin lines, an optically thin continuum, and a simple

emission geometry that results in the emission either completely filling the beam or filling some fraction of the beam in a well-defined way. In this scenario, the molecular column density can be calculated either through the adoption of an excitation temperature or through rotation diagram analysis using multiple lines (e.g., Goldsmith & Langer 1999, Najita et al. 2003). The calculations can be done using disk-averaged fluxes to derive a disk-averaged column density, or spatially resolved fluxes to derive a column density profile. A modified method can be used when the lines are marginally optically thick (Najita et al. 2003, Loomis et al. 2018b). Column densities can also be derived by fitting disk spectra assuming LTE and adopting some intrinsic linewidth, including the fitting of hyperfine lines in high-resolution spectra (Kastner et al. 2014, Bergner et al. 2019, Hily-Blant et al. 2019, Teague & Loomis 2020). For many lines detected in the (sub)millimeter regime, this LTE retrieval approach is valid as long as the molecular column densities vary slowly with radius and the lines originate below the disk atmosphere, where the gas density exceeds the line critical density.

In cases where LTE cannot be assumed, a limited forward modeling approach is needed to predict line excitation using the local disk density and temperature as well as molecular collisional excitation coefficients. Cases where lines are likely in non-LTE include millimeter observations of the disk atmosphere and rovibrational lines. A common approach in these cases is to use an LVG (Large Velocity Gradient) approximation (Piétu et al. 2007, van der Tak et al. 2007) or Monte Carlo–based radiative transfer codes (Brinch & Hogerheijde 2010, Hogerheijde & van der Tak 2000) coupled with an observation simulator to extract molecular abundances. The disk abundance structure can be parametric (e.g., Qi et al. 2011) or the product of a disk chemistry code (Bruderer et al. 2012, Du et al. 2015, Cleeves et al. 2018), but in either case the retrieval is achieved by quantifying the goodness of fit of the different abundance structures to the observations. For IR lines, fast line ray tracers can also be coupled to thermochemical codes to predict the rich line emission from disk regions with large velocity gradients (Pontoppidan et al. 2009, Bosman et al. 2017, Woitke et al. 2018). In addition to molecular abundances, these kinds of retrieval methods are also used to constrain disk environmental parameters such as gas mass, thermal structure, CO depletion, elemental ratios, and ionization (Piétu et al. 2007, Kamp et al. 2010, Dutrey et al. 2014, Cleeves et al. 2015b, Anderson et al. 2019, Miotello et al. 2019, Woitke et al. 2019).

Finally, we note that, in all these cases, retrievals rely on detailed spectroscopic data for the observed molecular lines, which are provided in databases such as HITRAN (Gordon et al. 2022), the Cologne Database for Molecular Spectroscopy (Müller et al. 2001, 2005; Endres et al. 2016), the Jet Propulsion Laboratory spectral line catalog (Pickett et al. 1998), and the Leiden Atomic and Molecular Database (Schöier et al. 2005). These, in turn, rely on laboratory experiments and computations.

3.3. Disk Molecular Inventories

There are 31 detected molecules in disks (not counting isotopologues), most (26) of which are presented by McGuire (2022, and references therein), with recent additions from Booth et al. (2021a), Canta et al. (2021), Phuong et al. (2021), and Brunken et al. (2022). Most (24) of these molecules were detected at millimeter wavelengths, followed by IR (10) and FIR (6). **Figure 3** shows these molecules and their observed isotopologues [also presented by McGuire (2022), except for $^{13}CO_2$ (Grant et al. 2022) and $HC^{18}O^+$ (Furuya et al. 2022)], organized into seven chemical "families": inorganic neutrals (excluding CO and S molecules), CO isotopologues, molecular ions, nitriles and isonitriles, hydrocarbons, O-containing organics, and S molecules.

IR observations have resulted in large disk samples with detections of gas-phase inorganic neutrals (H_2, OH, H_2O, CO, ^{13}CO, $C^{18}O$, $C^{17}O$, NH_3, and CO_2), the small organics HCN and

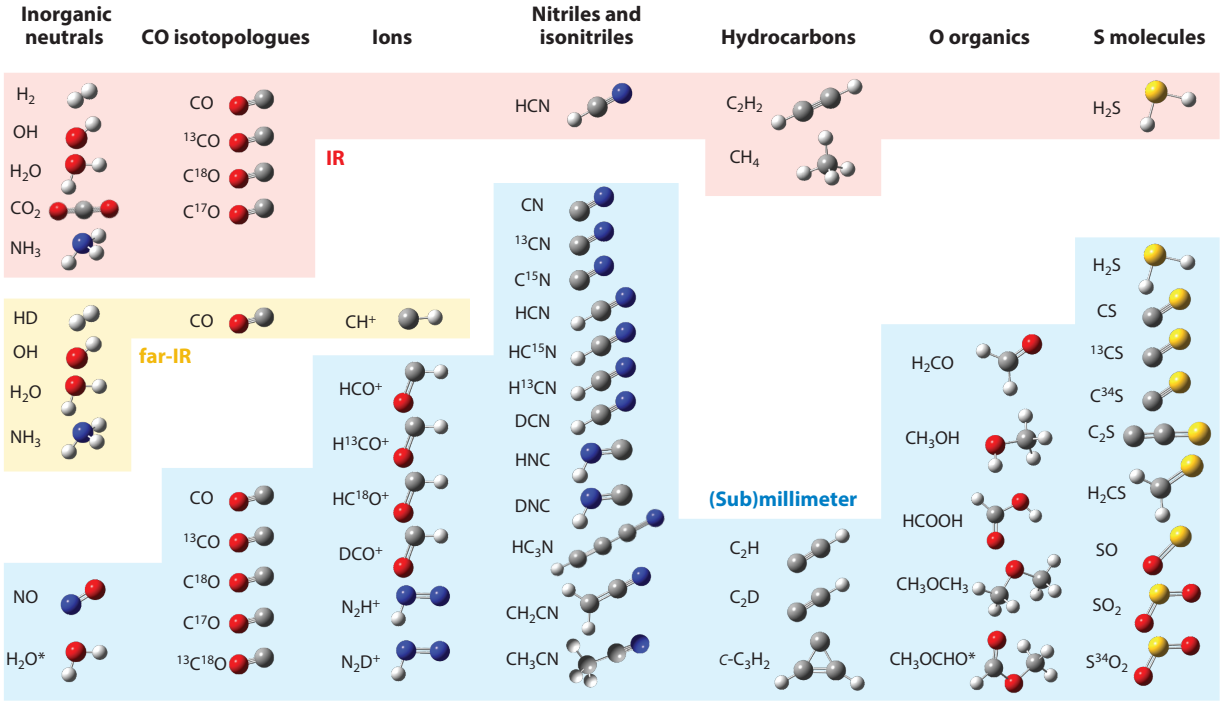

Figure 3

Illustration of the molecules detected so far in disks at IR (*red*), far-IR (*yellow*), and (sub)millimeter (*blue*) wavelengths. Asterisks indicate tentative detections.

C_2H_2, and H_2S (e.g., Lahuis et al. 2007, Carr & Najita 2011, Mandell et al. 2012, Najita et al. 2021). Together, they can be used to constrain the inner disk chemistry. In addition to narrow gas emission and absorption lines, IR spectra toward some disks contain features of PAHs (Acke et al. 2004, Geers et al. 2006) and of ice-phase H_2O, CO_2, and CO (Pontoppidan et al. 2005, Aikawa et al. 2012). We expect both the gas and ice IR inventory to grow rapidly in the coming years through JWST observations, and early JWST science has already presented one new inner disk molecule detection: $^{13}CO_2$ (Grant et al. 2022).

At FIR wavelengths, the only molecule detected toward more than a handful of objects is CO (Meeus et al. 2013). The few existing HD, OH, H_2O, and NH_3 detections provide unique constraints on disk physics and chemistry, however, and they have been the subject of numerous studies (e.g., Bergin et al. 2013, Fedele et al. 2013, Rivière-Marichalar et al. 2015, Salinas et al. 2016, van Dishoeck et al. 2021). This group of hydrides is important because they currently present the only constraints we have on cold water and ammonia in disks, and they provide a unique handle on the disk gas mass (HD).

Millimeter and submillimeter disk observations have resulted in a relatively large sample of CO isotopologue, HCO^+, HCN, and C_2H detections as well as $\gtrsim$10 detections of N_2H^+, DCN, CN, H_2CO, and CS (see Section 3.4). The remaining 28 molecules and isotopologues have been either rarely targeted (e.g., HNC) or rarely detected. A notable aspect of **Figure 3** is the prominence of the nitrile and isonitrile family, especially in comparison to O-bearing organics. This pattern can be compared with IR observations, where the detection rate of O-bearing molecules, nitriles, and hydrocarbons appears more balanced, indicating very different chemical environments in inner and outer disk regions.

3.4. Molecular Demographics

Molecular line detection rates and intensities across disk samples have provided the first measure of the diversity of chemical environments during planet formation, even though any interpretation is complicated by possible differences in line excitation. At FIR wavelengths, the detection rate has been too small to establish clear demographic patterns, although, for example, the low detection rate of water in T Tauri disks is in itself informative. This section therefore focuses on IR and (sub)millimeter constraints.

The inner disk molecular demographics probed by IR observations were reviewed by Pontoppidan et al. (2014) and have not been substantially revised since. Lines from water and small organics are common (30–50% detection rates with *Spitzer*) in disks around solar-type stars, and we speculate that these rates will increase to close to 100% with JWST. The detection rate is much lower for more massive stars and somewhat lower for cooler stars. In the latter case, there is evidence for a different disk chemistry based on distinct HCN/C_2H_2 ratios compared with more luminous stars (Pascucci et al. 2009, 2013). There is also evidence of a lower detection rate toward so-called transition disks, disks with a large central cavity, though the sample is small. These differences in line detections and intensities across different disk families may be due to different inner disk chemistry because of different levels of stellar irradiation, differences in line excitation, different levels of influx of icy pebbles, or a combination of all three (e.g., Salyk et al. 2011b, Pascucci et al. 2013, Antonellini et al. 2016, Najita et al. 2018, Banzatti et al. 2020). Distinguishing between these different explanations is currently complicated by the low spectral resolution and limited sensitivity of *Spitzer*, as well as by small observing windows of higher-resolution ground-based observations. Medium-resolution observations with JWST should directly address these difficulties, and a new demographic understanding of inner disk chemistry is likely forthcoming.

Millimeter line surveys of disks are not yet mature enough to enable determinations of detection rates and how they vary across populations. Instead, **Figure 4*a*** shows the distributions of reported disk-integrated fluxes normalized to 150 pc for a subset of commonly observed molecules using their brightest 1 mm transition (e.g., CO 2–1)[1]. These observations are from numerous publications (e.g., Öberg et al. 2010, 2011c, 2021b; Ansdell et al. 2016; Barenfeld et al. 2016; Guilloteau et al. 2016; Huang et al. 2017; Long et al. 2017; Miotello et al. 2019; Bergner et al. 2020; Pegues et al. 2021; Anderson et al. 2022). When interpreting these distributions, it is important to note that the line flux floor for each species is set by the survey sensitivity and hence is not very informative. The maximum fluxes for each species are informative, however, and show that the CO line is approximately an order of magnitude brighter than ^{13}CO, HCO^+, HCN, and CN, followed by $C^{18}O$, C_2H, and CS. N_2H^+, H_2CO, and DCN present the weakest emission among these commonly observed molecules. Many of the flux distributions are bimodal because of a focus in the literature on either small samples of large and bright disks (e.g., Dutrey et al. 2007, Bergner et al. 2020) or larger samples that are dominated by the more common smaller-sized and less bright disks (Ansdell et al. 2016, van Terwisga et al. 2019). Therefore, the range of observed line fluxes for a single species must be interpreted with caution, but it is still interesting to note that it frequently spans two orders of magnitude, indicating substantially different molecular reservoirs among planet-forming disks.

A similar source-to-source variation is observed among the small number of disks that have well-constrained column density radial profiles in multiple species. **Figure 4*b*** uses data from Qi et al. (2011, 2013, 2019), S. Zhang et al. (2018), Bergner et al. (2019,

[1]When a different line flux (e.g., CO 1–0 or 3–2) was reported, the 1 mm line flux was estimated under the assumption of optically thick emission for "bright" lines and optically thin emission for "weak" lines, and an excitation temperature of 20 K.

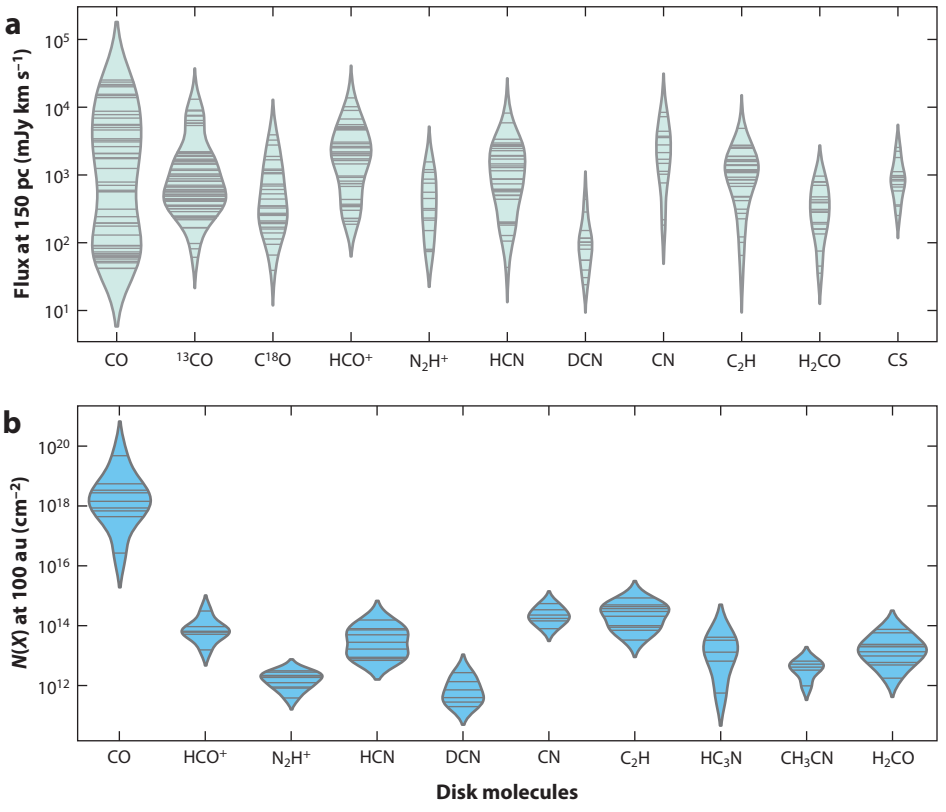

Figure 4

(*a*) Disk-integrated fluxes from 1 mm transitions, corresponding to ALMA B6, normalized to a distance of 150 pc. (*b*) Outer disk column densities extracted from spatially resolved ALMA observations. In these violin plots, the width of the distribution denotes the number of disks that fall within a certain flux or column density range, and each horizontal line signifies an individual measurement. Abbreviation: ALMA, Atacama Large Millimieter/submillimeter Array.

2021), K. Zhang et al. (2019, 2021), Cataldi et al. (2021), Facchini et al. (2021), Guzmán et al. (2021), Öberg et al. (2021a), Phuong et al. (2021), and Terwisscha van Scheltinga et al. (2021) to show the range in column densities at ∼100 au[2]. Even within this small and highly biased sample, there are orders-of-magnitude differences in column densities. Possible causes of this chemical diversity include differences in temperature structures, levels of CO freeze-out, high-energy radiation fluxes, disk ages, and initial chemical conditions across the disk sample. To obtain more detailed demographics, we need surveys that address the current sample biases and have the sensitivity to detect a range of molecular abundances.

3.5. Molecular Substructures

Within both the inner and outer disk regions we expect chemical substructure due to gradients in radiation flux, ionization, and temperature, as well as dust and gas surface density gaps and rings (Section 1.2). Analogous to dust substructures, which can be identified both through

[2]For two disks where 100 au data were not available, we use reported column densities at 70 and 240 au.

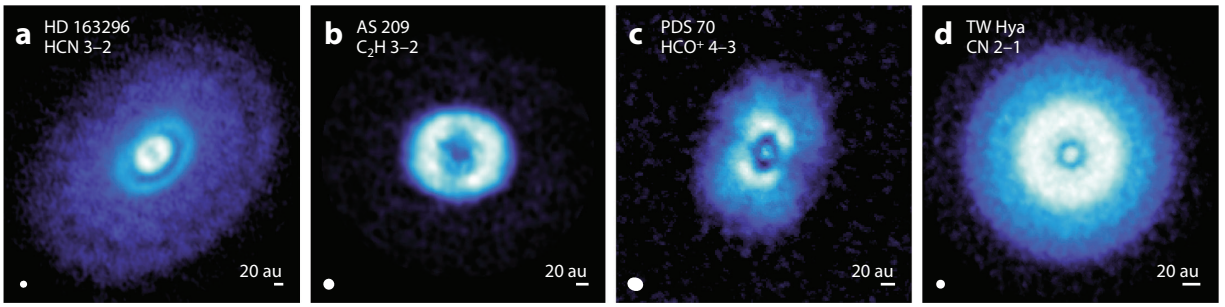

Figure 5

Examples of chemical substructures toward disks showing (*a*) the four rings in HCN emission toward HD 163296; (*b*) a single broad ring in C_2H emission toward AS 209; (*c*) a ring and a central peak in HCO^+ emission toward PDS 70; and (*d*) a ring, a plateau, and a central peak in CN emission toward TW Hya. The scale bar at the bottom right of each panel signifies 20 au; the oval at the bottom left represents the synthesized beam. Panels *a* and *b* adapted from Öberg et al. (2021b). Panel *c* adapted from Facchini et al. (2021). Panel *d* adapted with permission from Nomura et al. (2021); copyright 2021 AAS.

resolved images and through modeling of spectral energy distributions (Andrews 2020), molecular substructures can be observed through chemical imaging (**Figure 5**) and line excitation analysis. Furthermore, in a Keplerian disk, the spectral line shape can be used for spectroastrometry and to map different spectral line regions to different disk radii, providing additional tools to characterize chemical disk structures at smaller scales than are accessible with imaging alone.

Spectroastrometry, line excitation modeling, and spectral profile analysis of spectrally resolved lines have been especially important in accessing substructure in the inner disk (e.g., Pontoppidan et al. 2008, Najita et al. 2010, Fedele et al. 2013, Thi et al. 2014). Three examples of how line excitation and line spectral profiles can reveal chemical substructure are (*a*) the finding by Salyk et al. (2011b) that OH, C_2H_2, HCN, CO_2, and H_2O have different excitation temperatures, suggesting a radially progressive inner disk composition; (*b*) an observed trend between CO-emitting radii and stellar luminosity based on CO spectral profiles (Pontoppidan et al. 2011, Salyk et al. 2011a); and (*c*) the discovery of a radially varying H_2O/CO ratio based on a combination of excitation and spectral profile analysis (Banzatti et al. 2022). Spectral line profile analysis has also been applied to millimeter line observations to map out the molecular emission structure in disks (e.g., Dutrey et al. 2008, Rosenfeld et al. 2012, Bosman et al. 2021c). Such analyses have revealed gas and/or CO chemistry substructure on scales of a few astronomical units, spanning the radial gap between typical IR and millimeter substructure constraints.

Most millimeter-wavelength evidence for chemical substructure comes from spatially resolved observations using millimeter interferometers. Early examples include the discoveries of an H_2CO ring toward DM Tau (Aikawa et al. 2003), a DCO^+ ring toward TW Hya (Qi et al. 2008) and C_2H rings toward several disks (Henning et al. 2010). Higher-resolution images emerged with the arrival of ALMA, and ∼10 disks have been chemically characterized at scales of 0″.1–0″.2. Among these disks, chemical substructure is ubiquitous. The ALMA Large Program MAPS alone, which surveyed five disks, identified ∼250 rings, gaps, and shoulders (Law et al. 2021a). **Figure 5** illustrates the diversity of chemical substructures that have been observed, ranging from single rings to four-ringed systems, with ring and gap widths ranging from unresolved (<20 au) to hundreds of astronomical units.

There are multiple possible origins of the observed inner and outer disk chemical disk structures. The (gas-phase) formation and destruction of some species are temperature sensitive, which should result in peak abundances at certain disk radii. This temperature dependence may explain

some of the inner disk chemical differentiation as well as broader chemical rings in the outer disk. Similarly, molecules that depend on photochemistry for formation or destruction should vary across the disk because of a decreasing UV flux with disk radius, which may also cause observable chemical substructure (e.g., Cazzoletti et al. 2018, Bergner et al. 2021). Another potential cause of substructure is snowlines (see Section 4.1), though they have been excluded as explanations for most of the currently observed dust and molecular substructures (Huang et al. 2018b, Long et al. 2018, Law et al. 2021a). Finally, gaps in dust and gas may produce chemical substructure as a result of enhanced photochemistry in dust gaps (Bosman et al. 2021a), different thermal structures in dust gaps and rings (Facchini et al. 2018b, Alarcón et al. 2020), decreased grain surface chemistry in dust gaps, and lower molecular gas column densities in (H_2) gas gaps (Teague et al. 2017). Observational tests of these proposed relationships are somewhat ambiguous. There is no one-to-one correspondence between dust and chemical structures (Jiang et al. 2022), but, as shown in **Figure 6**, there are some coincidences between dust and chemical substructures, suggesting that specific dust gap and ring properties may be needed to shape the chemical structures of disks. Conversely, it may be possible to use molecular emission substructure as a probe of disk gap and ring properties, including whether a gap is formed by a planet (Bergner et al. 2019). In addition,

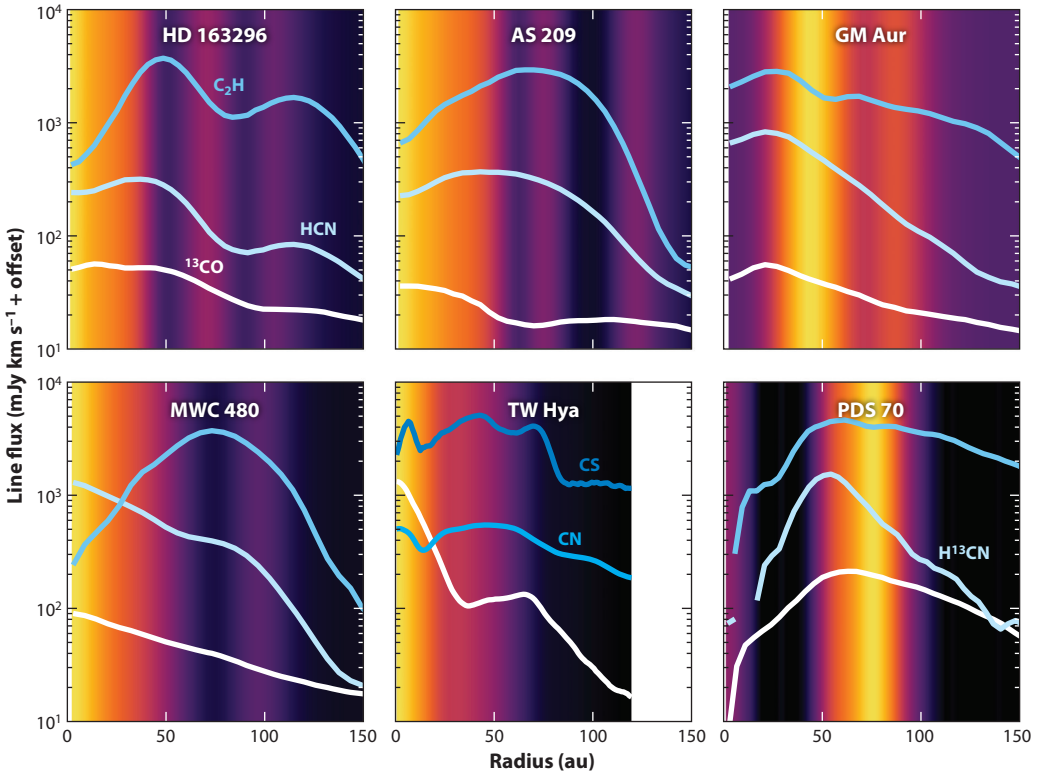

Figure 6

Comparisons of dust substructure (*background*) and molecular emission radial profiles (*lines*) toward six disks (Facchini et al. 2021, Law et al. 2021a, Nomura et al. 2021). The beam size of the dust and lines has been homogenized and is between 10 and 25 au toward the different disks.

these observations suggest that the local chemical environment within which a planet assembles could be quite distinct from the chemistry at nearby disk radii.

3.6. Vertical Chemical Gradients and Substructure

As discussed in Section 1.3, the disk chemistry is vertically highly structured. In the disk atmosphere, molecular abundances are regulated by photodissociation, which results in molecule-specific and, for CO and N_2, isotopologue-specific photodissociation fronts (e.g., Visser et al. 2009, Miotello et al. 2014). Toward the disk midplane, molecular abundances are bounded by vertical condensation fronts or snow surfaces, though a combination of turbulence and nonthermal desorption may also maintain a small amount of volatiles in the coldest part of the disk midplane (e.g., Hersant et al. 2009). As a result, most molecules should be present in distinct vertical layers, which together constitute the disk "molecular layer" (Aikawa et al. 2002). Characterizing the resulting vertical chemical stratification is key to benchmarking disk chemistry models and constraining the overall disk chemistry evolution.

At (sub)millimeter wavelengths, interferometers provide high enough angular resolution to spatially resolve vertical gradients in bright molecular line emission, and by exploiting the position and velocity information, one can reconstruct the full 3D tomography of the line intensity (Dutrey et al. 2017, Teague et al. 2020). **Figure 7** shows a textbook case of CO and CS emitting from different layers in the edge-on disk named the Flying Saucer (Dutrey et al. 2017), where the lack of CO emission in the disk midplane is explained by CO freeze-out. The emission of CS 5–4 originates from a $z/r \sim 0.1$ layer, close to the disk midplane, demonstrating that the molecular layer can extend deep into the disk. Emission surfaces can also be extracted for disks at other inclinations by exploiting the Keplerian rotation pattern and disk geometry (Pinte et al. 2018a). This methodology requires high angular resolution and a high signal-to-noise ratio; therefore, it has been applied only to particularly bright, optically thick molecular lines. As a consequence, disk (front-side) emission heights exist for ^{12}CO toward a fairly large sample, for rare CO isotopologues toward a handful of sources, and for other molecules toward even fewer disks (Huang et al. 2020; Law et al. 2021b, 2022; Paneque-Carreño et al. 2022). In these sources, CO (isotopologue) emission becomes optically thick at a range of z/r, indicating that the extent of the warm molecular layer and the CO abundance vary substantially between disks. The molecular

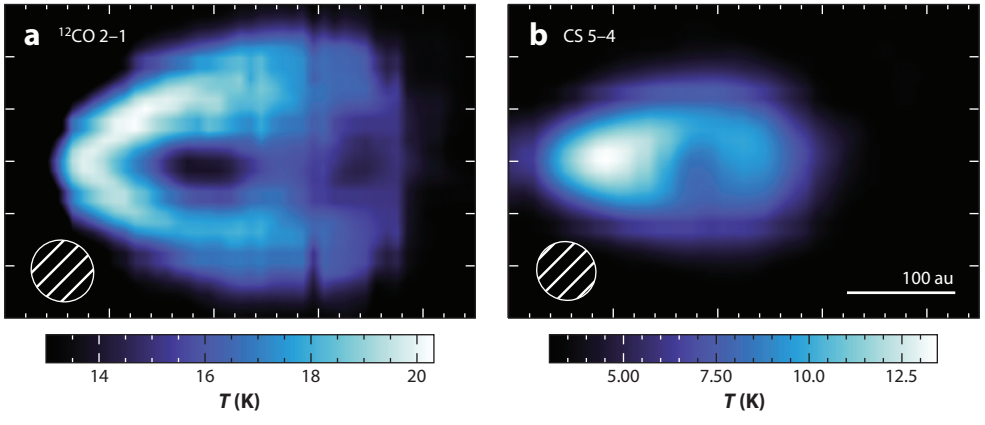

Figure 7

Tomographically reconstructed distribution of (*a*) ^{12}CO and (*b*) CS in the Flying Saucer. Figure adapted with permission from Dutrey et al. (2017, figure 6); copyright 2017 ESO.

emission height derived from the disk backside should trace the snow surface, but that has only been achieved for CO toward three disks so far, though this technique is under active development (Pinte et al. 2018b, Casassus et al. 2021, Izquierdo et al. 2022). Of the other molecules that have been characterized, CN is present at high elevations in the disk atmosphere, which is consistent with CN formation through reactions between UV-pumped H_2 and atomic N (Cazzoletti et al. 2018). Other small organics, especially HCN, reside closer to the planet-forming midplane.

For cases where direct imaging of vertical chemical structures is impractical or impossible—which include inner disk line observations as well as weaker (sub)millimeter lines emitting in the outer disk—line excitation analysis offers an alternative approach to characterize the disk vertical chemical structure as long as the disk temperature structure is constrained. So far, this approach has not been extensively used in the inner disk because of large uncertainties in the vertical temperature gradient, but this may soon change as medium-resolution JWST disk spectra analysis techniques are developed. The chemistry of the warm and highly irradiated disk atmosphere of the outer disk has been probed by high-J CO lines and by the atomic O line at 63 μm (Bruderer et al. 2012, Kamp et al. 2013). The excitation temperatures of other small and midsized molecules have been retrieved from medium and high spatial resolution data, and at 15–40 K they are consistent with models of the disk midplane and molecular layer (Loomis et al. 2018a, Bergner et al. 2019, Cataldi et al. 2021, Facchini et al. 2021, Guzmán et al. 2021, Ilee et al. 2021, Pegues et al. 2021). Interestingly, the excitation temperatures of several complex organic molecules (COMs), including CH_3CN, place them close to the midplane at $z/r \sim 0$–0.2 (Loomis et al. 2018a, Ilee et al. 2021), suggesting that they may contribute to the organic budget of forming planets. Interpretation of such data is complicated, however, by the possibility of non-LTE excitation; for example, for CN there is a range of derived excitation temperatures and inferred emission heights (Chapillon et al. 2012, Hily-Blant et al. 2017, Teague et al. 2020).

4. THE DISTRIBUTIONS AND CHEMISTRY OF DISK VOLATILES

The distributions of volatiles in disks, including volatile organics, provide the initial conditions for planet volatile compositions and chemistry. Perhaps the most important concept used in predicting these distributions is the condensation front, or snowline, which is introduced in Section 4.1. Section 4.2 reviews the existing observational evidence for how the major volatile elements O, C, N, S, and P are distributed across the disk. Section 4.3 focuses on the volatile organics in disks and on the importance of inheritance and in situ UV chemistry for disk organic reservoirs. Stable isotope ratios are an important tool used to trace the origins and evolution of volatiles in disks; Section 4.4 presents observed disk isotopologue ratios and the associated constraints on isotope fractionation chemistry.

4.1. Snowlines

Volatile condensation fronts are briefly discussed in Sections 3.5 and 3.6 as causes of chemical substructure and vertical chemical gradients. In this section, we focus on the radial dimension (i.e., on snowlines) and review the theory and observations that have been developed to predict and constrain snowline locations. These locations matter for several reasons. First, freeze-out of major volatiles changes both the gas and grain surface chemical trajectories. For example, freeze-out of CO enables the formation of O-rich organics in the ice and may promote a C-rich gas-phase organic chemistry (e.g., Walsh et al. 2015, Schwarz et al. 2018). Second, in planet formation models, snowlines of major carriers of O, C, and N determine the volatile compositions of primary atmospheres and planetary envelopes, and they have emerged as a major explanatory framework for observed exoplanet atmospheric compositions (Öberg et al. 2011a, Cridland et al. 2020). Third,

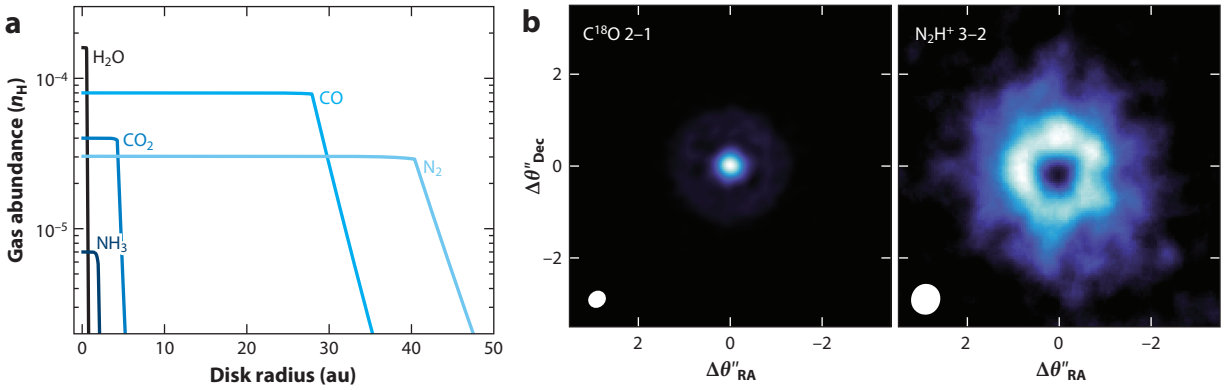

Figure 8

(*a*) Expected gas-phase abundances of five major CNO carriers in the disk midplane, assuming a simple T Tauri disk temperature model and inheritance of interstellar volatiles. The sharp abundance overturns mark the respective snowlines. (*b*) Observations of $C^{18}O$ and N_2H^+, with ALMA toward TW Hya. Both the outer edge of $C^{18}O$ and the inner edge of the N_2H^+ should trace the CO snowline. Data are from Qi et al. (2013) and Calahan et al. (2021b). Abbreviation: ALMA, Atacama Large Millimeter/submillimeter Array.

snowlines, especially the water snowline, are also expected to affect dust grain evolution (e.g., Gundlach & Blum 2015, Okuzumi & Tazaki 2019) and may regulate when and where planet cores assemble and, hence, the formation locations of terrestrial planets versus Neptune-like planets and gas giants (Drazkowska et al. 2022).

Figure 8*a* illustrates the five major snowline locations in a generic disk model for a solar-type star, using the disk framework, binding energies, and abundances from Öberg & Wordsworth (2019) and Öberg & Bergin (2021), except that we adopt a midplane temperature profile with $T_{1au} = 150$ K and a power of −0.47. This simple parametric model provides a useful starting point for discussing snowline locations, but it is important to keep in mind that it presumes a specific temperature profile that is not generally applicable and that, in reality, snowline models are complicated by a range of dynamical and chemical effects. To begin, the disk temperature structure changes over time, sometimes abruptly due to an accretion burst. Such accretion bursts move snowlines outward, while stellar evolution results in an inward migration of snowline locations over time (Ciesla & Cuzzi 2006, Banzatti et al. 2015, Cieza et al. 2016, Price et al. 2021). Furthermore, inward drift of pebbles often occurs on timescales similar to those of desorption, which can readily move the effective snowline inward by a factor of two (Piso et al. 2016). Snowline locations also depend on the chemical compositions of icy grains, since volatile binding energies depend on the grain surface material (e.g., Collings et al. 2003, Fayolle et al. 2016, Kamp et al. 2017, Potapov et al. 2018). In addition, H_2O and CO_2 ices can entrap hypervolatiles, effectively producing two snowlines: one at the expected location and one at the location where the ice matrix desorbs or crystallizes (Bar-Nun et al. 1985, Lunine & Stevenson 1985, Collings et al. 2004, Simon et al. 2019). The impact of snowlines on gas and solid abundances is also more complex than shown in **Figure 8*a***, which considers only a balance between desorption and adsorption. If the disk is somewhat turbulent, then gas diffusion should result in the depletion of vapor inside the snowline and a buildup of ice outside the snowline (e.g., Cuzzi & Zahnle 2004, Ros & Johansen 2013, Krijt et al. 2016). Finally, the inherited volatiles may chemically evolve over the disk lifetime (Eistrup et al. 2016, Schwarz et al. 2018), which will change the abundances of volatiles and therefore the relative importance of different snowlines.

Snowline locations have been observationally constrained through at least six different techniques: (*a*) images of major volatiles with important snowlines, (*b*) images of gas-phase chemical

tracers (**Figure 8**), (*c*) tomography using spectrally resolved lines (Carr et al. 2018, Salyk et al. 2019), (*d*) line excitation studies (K. Zhang et al. 2013, Blevins et al. 2016), (*e*) changes in dust spectroscopic properties at a snowline (Cieza et al. 2016), and (*f*) association of disk dust substructures with snowlines (K. Zhang et al. 2015). Each of these techniques has advantages and disadvantages. Direct imaging of snowlines is currently possible only for CO by use of rare isotopologues, and even for CO it is often unclear whether the observed drop-off in CO vapor corresponds to the CO snowline, a decrease in C and O elemental abundances, or an overall decrease in gas surface density. There are plausible gas-phase chemical probes of H_2O, CO, and N_2 snowlines that can be used to extract snowline locations (Qi et al. 2013, 2019; Bjerkeli et al. 2016; Leemker et al. 2021), but these probes are not always unique to depletion of the targeted volatile at its snowline and therefore require careful interpretation (van 't Hoff et al. 2017). Spectral tomography (the estimation of the spatial distribution from spectral information, taking advantage of Keplerian rotation) of snowlines is limited by the possible presence of non-Keplerian motion. Furthermore, the water IR spectral lines that are accessible from the ground, and hence at high spectral resolution, are not well matched to snowline excitation conditions. Snowline constraints from line excitation depend on the assumed disk temperature structure, which is often uncertain. The fifth approach, observing changes in dust spectroscopic properties across snowlines, depend on models of, for example, increased fragmentation at major snowlines; therefore, they are quite indirect. Finally, a proposed association between disk dust substructure and snowlines has not yet been demonstrated. As a result, this approach remains highly speculative (Huang et al. 2018b, Long et al. 2018). Given the inherent uncertainties in all these techniques, a snowline location should ideally be observed using at least two different methods in order to be considered secure.

4.2. Elemental O, C, N, S, and P Disk Abundances

The elemental abundances of O, C, N, S, and P across disks regulate the volatile compositions of forming planets and planetesimals. At least four factors influence the O, C, N, S, and P abundance patterns: the nature of the O, C, N, S, and P carriers inherited from the interstellar and protostellar phases, chemical transformations in the disks, locations of condensation fronts, and transport processes. In this section, we review existing constraints on elemental O, C, N, S, and P disk abundances, organized by disk location (outer versus inner disk) and phase (solid versus gas). We proceed from the expected least-processed (outer disk solids) to most-processed volatiles (inner disk gas), but we note that efficient radial and vertical transport may blur the distinctions between processed and pristine volatile reservoirs in disks.

In the outer disk, O, C, N, S, and P are present in both refractory and icy solids. O is a major component of silicates, which are observed to be abundant in disks. On the basis of comet observations (Altwegg et al. 2019), refractory C is also abundant and may be inherited from the ISM, a product of disk organic chemistry, or a combination of both. Some evidence from observed high gas-phase C/O ratios suggests that a portion of this refractory C reservoir is transformed into C gas during the disk lifetime (Bosman et al. 2021b). N is often assumed not to have a significant refractory phase, but recent cometary measurements, as well as previous interstellar ice spectroscopy, suggest that ammonium salts may be an important carrier of N (Boogert et al. 2015, Altwegg et al. 2020).

The outer disk ice reservoir is constrained by interstellar ice observations (setting the initial conditions), a small set of disk ice observations (e.g., Pontoppidan et al. 2005, Aikawa et al. 2012), comet compositions (Mumma & Charnley 2011, Altwegg et al. 2019), and disk gas-phase observations of sublimated ice. Such disk gas-phase observations are possible following a stellar luminosity burst and in sources where the outer disk is exposed to high levels of stellar radiation due to the

combination of a higher-mass star and a large inner cavity (Banzatti et al. 2012, 2015; Cieza et al. 2016; Lee et al. 2019; Booth et al. 2021b; van der Marel et al. 2021). Disk and comet observations indicate that, similar to the ISM, disk icy grains consist mainly of H_2O, CO_2, CO, NH_3, and O-rich organics. On the basis of theory, we also expect N_2 to be present in the coldest disk regions. H_2O ice is probably inherited largely from the ISM, as suggested by models (e.g., Visser et al. 2009) and Solar System H_2O D/H ratios (Cleeves et al. 2014), while the contribution of inheritance versus in situ chemistry to the other major O, C, and N carriers is less well constrained. The outer disk ices also appear to contain substantial amounts of S (Altwegg et al. 2019, Booth et al. 2021a) as well as some P (Altwegg et al. 2019), though most S and P are expected to be present in refractory carriers (see the paragraph below on inner disk S and P).

Some aspects of the outer disk gas OCNSP composition can be directly constrained through observations of CO, H_2O, and NH_3, the three expected major carriers that are observable at FIR and millimeter wavelengths. CO chemical gas often appears to be depleted in disks (see Section 5.1), reducing the C and O gas abundances. This may be explained by a combination of CO processing into less volatile species and dynamics (Schwarz et al. 2018, Krijt et al. 2020). H_2O vapor has been detected in only one T Tauri disk and a handful of Herbig Ae disks, providing independent evidence that the outer upper disk layers are generally dry and therefore O-poor (Hogerheijde et al. 2011, Meeus et al. 2012, Du & Bergin 2014, van Dishoeck et al. 2021, Pirovano et al. 2022), though the inferred H_2O depletion level does depend on the assumed disk structure and water excitation (Kamp et al. 2013). Finally, NH_3 has been observed in only one disk (Salinas et al. 2016), and its contribution to the outer disk N reservoir remains rather unclear. There have been no observations of P-bearing species in disks, and observations of gas-phase S molecules, such as CS and H_2S, indicate that less than 1% of S is in the gas phase (Phuong et al. 2018, Le Gal et al. 2021, Rivière-Marichalar et al. 2022) and, hence, that 99% is present in refractory grains and ices. Additional, more indirect constraints on the outer gas composition originate from observations of chemical probes of gas-phase elemental C/O ratios, such as C_2H/CO and CS/SO abundance ratios (Cleeves et al. 2018, Miotello et al. 2019, Fedele & Favre 2020, Le Gal et al. 2021). These studies confirm that the outer disk gas is depleted in O, resulting in enhanced C/O ratios that can exceed unity (Bosman et al. 2021b). Disks may also be somewhat depleted in C, while there has been no indication of N depletion, implying supersolar N/O and N/C ratios in the outer disk gas (Cleeves et al. 2018).

In the inner disk, the solid composition is constrained by disk IR spectroscopy of silicates, gas-phase abundances inside of refractory dust sublimation fronts, and Solar System abundance patterns. According to IR spectroscopic observations, silicate grains are an important O carrier in the inner disk (van Boekel et al. 2004, Natta et al. 2007, Bouwman et al. 2008), while the abundance of refractory C is less clear. The Solar System record suggests that the inner Solar Nebula solids were C-poor, and observations of low C/O ratios on white dwarfs polluted by infalling planet debris indicate that C-poor solids in inner disk regions are a general phenomenon (Lodders 2003, Wilson et al. 2016). The N content of inner Solar System solids also appears to have been low. By contrast, meteoritic measurements suggest that almost all P and approximately half of S are present in refractory grains in inner disks (Lodders 2003). The abundance of refractory S in inner disks has also been estimated through observations of S elemental abundances in accretion flows onto Herbig Ae stars, confirming that it is present mainly in refractory grains in disks (Kama et al. 2019).

In the inner disk, all O, C, and N not bound up in refractory grains are expected to be present in the gas phase. The major O and C carriers, H_2O, CO, and CO_2, are directly accessible in the inner disk atmosphere through IR observations, while the major N carrier, N_2, is not, and NH_3 is present at low abundances (Pontoppidan et al. 2019, Najita et al. 2021). The inferred gas

composition around solar-like stars is generally dominated by CO and H_2O (Pontoppidan et al. 2014), but the gas-phase C/O ratio is currently not well constrained and may vary substantially between disks due to different levels of icy pebble flux and sequestration of water in the outer disk (Najita et al. 2011, Banzatti et al. 2020). To date, S and P carriers have not been detected in the inner disk gas. Finally, note that the link between the observed disk atmospheric abundances and midplane reservoirs is not obvious.

Combining the above constraints, the inner disk refractory solids appear C- and N-poor and O-, S-, and P-rich. The inner disk gas composition varies between disks and likely depends on a combination of local processes and the influx (or lack thereof) of icy grains from the outer disk. As a result, it may present a range of C/N/O ratios. In the outer disk, the icy solids are initially O-dominated, but they become more and more enriched in C and N toward the outermost disk regions, where the most volatile C and N carriers (CO, small hydrocarbons, and N_2) freeze out. Conversely, the gas is generally O-poor, but it also appears somewhat depleted in C, probably due to CO depletion through a combination of freeze-out, grain dynamics, and chemical conversions. Only in the outermost disk would we expect the gas to also be depleted in N_2 because of the presence of N_2 snowlines (Qi et al. 2019).

4.3. Organic Disk Chemistry

Access to organic feedstock molecules constitutes a key aspect of chemical habitability. Disk organic molecules can be delivered to terrestrial planets through impacts of planetesimals that originate in both the inner and outer disk regions, as well as through accretion of a primary atmosphere from the local disk gas, which motivates explorations of organic chemistry across all disk radii. Protoplanetary disks serve both as conduits of the inherited interstellar and protostellar organic chemistry to planets and planetesimals and as active producers of new organic molecules using the disk inorganic and organic C reservoirs. This combination of inheritance and local organic chemistry results in a distribution of organics in disks that is complicated and evolves over time.

Carbon enters the disk in the form of volatile inorganic and organic gas and ice (e.g., CO and CH_3OH) and more refractory large aromatic and aliphatic hydrocarbons, PAHs, and C grains. In the chemically active layers of the disk, some of the inherited refractory C may be vaporized and feed a C-rich top-down gas-phase organic chemistry (Siebenmorgen & Heymann 2012, Bosman et al. 2021b). What remains provides disks with a unique organic reservoir that is characterized by aromatic groups and relatively low levels of O, especially in comparison to inherited organic ices. Interstellar and protostellar ices often contain high abundances of simple organics in the forms of CH_4, CH_3OH, and perhaps HCOOH (Öberg et al. 2011a, Boogert et al. 2015). These can be energetically and nonenergetically processed to form COMs (Bernstein et al. 2002, Muñoz Caro et al. 2002, Öberg et al. 2015a, Chuang et al. 2017, Jørgensen et al. 2020, Ioppolo et al. 2021). Importantly, this complex organic chemistry takes place in an O-rich environment (i.e., the H_2O-, CO-, and CO_2-dominated ice mantle) and therefore tends to favor the production of O-rich organics such as alcohols, organic acids, aldehydes, ethers, and ketones. Early evidence for the inheritance of interstellar and protostellar ices came from Solar System observations of comet organics, which have an O-rich contingent (Mumma & Charnley 2011); this evidence is supported by more recent comparisons between comet and protostellar inventories (e.g., Drozdovskaya et al. 2019). O-bearing organics that likely originate from interstellar or protostellar ice sublimation have also been observed in young disks (van 't Hoff et al. 2018a, Lee et al. 2019, Podio et al. 2020). The strongest evidence to date for substantial inheritance of interstellar and protostellar ice chemistry has come from recent observations of gas-phase CH_3OH and COMs in disks that are too warm to sustain CH_3OH production from CO ice (Booth et al. 2021a, van der Marel et al. 2021, Brunken et al. 2022), the major CH_3OH production channel in the ISM (Tielens & Hagen

1982, Hidaka et al. 2004, Fuchs et al. 2009). Therefore, the observed COMs in these disks are inferred to have originated from sublimation of inherited organic ices. Such ices can be further processed in disks when icy grains are lofted up from the relatively chemically inert midplane into the disk upper layers (Ciesla & Sandford 2012, Bergner & Ciesla 2021). In either case, icy planet building blocks should generally contain substantial amounts of O-rich complex organics.

Most current inner and outer disk observations probed the gas compositions of disk layers with relatively short chemical timescales (e.g., Henning et al. 2010), where detected organics are products of disk in situ organic chemistry. This chemistry is powered by high temperatures and high-energy radiation in the inner disk and by high-energy radiation (UV and X-rays) alone in the outer disk (e.g., Agúndez et al. 2008, Semenov & Wiebe 2011, Walsh et al. 2015, Bergner et al. 2019, Bosman et al. 2021b). As reviewed in greater detail by Henning & Semenov (2013), the presence of the small organics C_2H_2, HCN, and CH_4 in the inner disk is generally consistent with a high-temperature gas chemistry (e.g., Willacy & Millar 1998, Ilgner et al. 2004, Walsh et al. 2015, Najita & Ádámkovics 2017). Efforts to explore the roles of irradiation fields, detailed radiative transfer, nonsolar elemental ratios, transport, and grain–gas interactions on inner disk organic abundances are underway (e.g., Bruderer et al. 2015, Najita & Ádámkovics 2017, Woitke et al. 2018, Wei et al. 2019, Price et al. 2020, Anderson et al. 2021, Duval et al. 2022). It is already clear, however, that this inner disk chemistry produces a gas-phase organic reservoir in the terrestrial planet-forming zone that is completely different from those in the outer disk and the ISM.

In the outer disk, C_2H, HCN, and H_2CO have been widely detected in sources across a range of stellar masses and ages (Bergner et al. 2019, Pegues et al. 2020, Guzmán et al. 2021). Larger organics, such as HC_3N, c-C_3H_2, and CH_3CN, are also commonly detected (Chapillon et al. 2012, Öberg et al. 2015a, Bergner et al. 2018, Ilee et al. 2021). High spatial resolution, multiline observations have located these larger nitriles and hydrocarbons in the disk molecular layer (Ilee et al. 2021, Öberg et al. 2021b). By contrast, larger O-containing organics are relatively rare, with only one detection of CH_3OH in a disk not obviously experiencing extensive ice desorption (Walsh et al. 2015). Outer disk in situ gas chemistry is then characterized by an O-poor and N-rich organic chemistry, consistent with other evidence of O-poor gas in outer disk layers (see Section 4.2). There is increasing evidence that this chemistry is qualitatively similar to that of classical PDRs (Jonkheid et al. 2004, Kamp & Dullemond 2004, Chapillon et al. 2012, Agúndez et al. 2018, Le Gal et al. 2019a). The organic products of this PDR-like and O-poor disk gas chemistry, including the prebiotically interesting nitriles, may become incorporated into planet atmospheres in the outer disk and also freeze out onto comet-forming pebbles. The latter scenario would provide planetesimals with a second reservoir of organics that is distinct from the inherited protostellar one, which may at a later stage be delivered to terrestrial planets through impacts. The importance of this reservoir would depend on a combination of the disk lifetime production of nitriles and the efficiency of downward transport of disk atmosphere chemistry products.

4.4. Isotope Fractionation Chemistry

Isotopic fractionation occurs at low temperatures due to small differences in zero-point energies between heavier and lighter molecules, as well as in the PDR-like disk regions due to isotopologue-specific photodissociation (e.g., Aikawa & Herbst 2001, Willacy 2007, Visser et al. 2009, Miotello et al. 2014). Isotopic fractionation patterns in molecules in disks are generally used either to assess the current thermal or irradiation environment or to link together different evolutionary phases (Ceccarelli et al. 2014). The first use case assumes fast chemical timescales such that observed D/H and other isotopic ratios reflect disk environmental conditions. This assumption is generally valid for gas-phase molecules in the disk atmosphere and intermediate vertical layers. The second use case makes the opposite assumption, such that the observed isotopologue ratio reflects

the environmental conditions of an earlier stage and can be used to infer inheritance. In disks, this assumption might hold for ices in the midplane, depending on the degree of vertical and radial mixing. This hypothesis could be tested through isotopic gas observations in disks where ice sublimation controls the gas abundances (Booth et al. 2021a), and perhaps also through ice observations of deuterated water with JWST. In the meantime, all our isotopic measurements in disks originate from the chemically active disk atmosphere and intermediate layers.

Five molecules, namely HCO^+, HCN, N_2H^+, HNC, and C_2H, have been detected in both deuterated and nondeuterated forms (Qi et al. 2008, Huang & Öberg 2015, Loomis et al. 2020). The last two have single detections, however, and are not further considered here. For HCO^+ and HCN, the disk-integrated D/H ratios are elevated above the cosmic D/H ratio by several orders of magnitude. This observation implies an active deuterium chemistry in the outer disk—deuterium fractionation of these and related species can occur through the cold H_2D^+ channel or the somewhat warmer CH_2D^+ channel, and both appear to be active in disks (e.g., Willacy 2007, Huang et al. 2017, Salinas et al. 2017, Aikawa et al. 2018, Cataldi et al. 2021). The D/H ratios in HCN and HCO^+ are quite similar, indicating a shared formation environment, while N_2H^+ is substantially more deuterated (**Figure 9**). The latter is expected if most N_2H^+ originates close to the cold disk midplane between the CO and N_2 snowlines (Aikawa et al. 2018). There is no clear

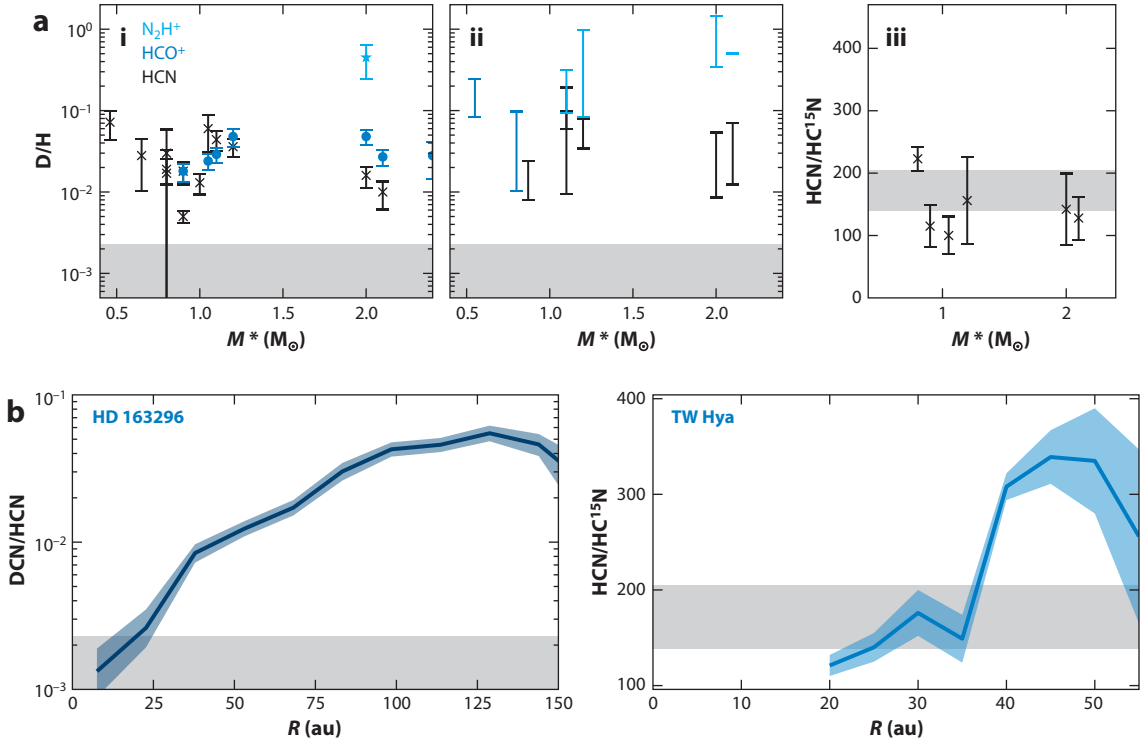

Figure 9

(*a*) Disk-integrated D/H ratios for HCN, HCO^+, and N_2H^+. (*i*) Disk-averaged values. (*ii*) Ranges extracted from spatially resolved observations. (*iii*) $^{14}N/^{15}N$ ratios for HCN toward a sample of protoplanetary disks. The shaded region depicts D/H values in comet volatiles and the range of $^{14}N/^{15}N$ in cometary HCN (Bockelée-Morvan et al. 2015, Altwegg et al. 2019). (*b*) Radially resolved DCN/HCN and HCN/$HC^{15}N$ ratios. Data in panel *a* are from Fuente et al. (2010), Teague et al. (2015), Guzmán et al. (2017), Hily-Blant et al. (2017, 2019), Huang et al. (2017), Salinas et al. (2017), Bergner et al. (2020), Cataldi et al. (2021), and Pegues et al. (2021). Data in panel *b* are from Hily-Blant et al. (2017, 2019) and Cataldi et al. (2021).

pattern in the degree of deuteration with stellar mass and luminosity, as might be expected from a cold-chemistry tracer. However, this lack of a pattern may be an effect of the present small and biased sample, which includes only hotter stars with large disks and, hence, substantial cool disk regions. Within individual disks, the D/H ratio in all three molecules generally increases with disk radius and hence with a decreasing disk temperature (Qi et al. 2008, Cataldi et al. 2021) (**Figure 9**), but the sample is still very small.

There are theoretical reasons to expect nonsolar C and O isotopologue ratios in disks (e.g., Miotello et al. 2016). Observations of ^{13}C isotopologues in disks exist for CO, HCO^+, HCN, CN, and CS, as do observations of ^{18}O and ^{17}O isotopologues for CO and observations of $HC^{18}O^+$ (see McGuire 2022 and references therein). In theory, fractionation in C and O could be extracted. In practice, doing so has proven difficult because of high or unknown optical depths of the main isotopologue lines. Instead, minor isotopologues are often used to constrain the optical depth of the major isotopologue, assuming local ISM isotopic ratios (e.g., Williams & Best 2014, Booth et al. 2019, K. Zhang et al. 2021). Two exceptions are studies by Smith et al. (2015), who used IR absorption line observations to derive a nonsolar $^{13}C/^{12}C$ in CO in inner disks, and by Yoshida et al. (2022), who used optically thin line wings of CO 2–1 transitions to measure a low $^{13}C/^{12}C$ ratio in CO in the outer disk of TW Hya. $^{15}N/^{14}N$ ratios have been extracted for HCN toward a handful of disks, and HCN is always enriched in ^{15}N. In the two disks with spatially resolved HCN fractionation observations, the $HCN/HC^{15}N$ ratio increases with radius; in other words, the disk gas is the most fractionated in ^{15}N close to the star (Hily-Blant et al. 2017, 2019; Guzmán et al. 2018). This behavior is the opposite of deuterium enrichment in HCN, and it strongly indicates that HCN enrichment in ^{15}N is due to isotopologue selective photodissociation (Heays et al. 2014), rather than cold isotope fractionation. In one disk, TW Hya, both CN and HCN fractionation in ^{15}N have been measured, and CN is much less enriched than HCN (Hily-Blant et al. 2017), indicating the presence of two different N reservoirs.

Isotopologue ratios could be used to assess disk chemistry contributions to comet inventories. In the case of HCN, the disk-averaged $^{15}N/^{14}N$ ratio is consistent with comet values, and for disks with radially resolved emission, disk values agree with comets in the inner tens of astronomical units of the disk (**Figure 9**), which is where most comets formed in the Solar System (Mumma & Charnley 2011). If disk fractionation chemistry is important for cometary isotopic ratios, the lower fractionation observed at larger disk radii should imprint on planetesimals assembling in the outskirts of disks, which could be tested by measuring $^{15}N/^{14}N$ in Solar System bodies that formed beyond 40 au. In the case of HCN D/H ratios, disk-averaged values are orders of magnitude higher than comet ratios, but radially resolved data have shown cometary D/H values in the inner 30 au in some disks (Cataldi et al. 2021). In summary, isotopologue ratios in disks and comets appear consistent, but that is not sufficient to ascribe a causal link between the two. More detailed data on the fate of disk gas-phase fractionation products, as well as disk chemistry models that take into account both dynamics and isotopic fractionation in ices, are needed to address this question (Faure et al. 2015). In addition, if disk H_2O and CH_3OH D/H values become available, a comparison between these and comet values would provide constraints on the relative contributions of inheritance and in situ disk chemistry for volatiles and small O-rich organics.

5. CHEMICAL PROBES OF DISKS AND PLANET FORMATION

Molecular observations often provide the best and sometimes the only path to constraining physical disk properties important for disk evolution and planet formation. Here we review chemical probes of disk gas mass and surface density (Section 5.1), ionization (Section 5.2), temperature (Section 5.3), and dynamics, including planet formation (Section 5.4). In each case, we provide

a brief overview of how disk chemistry and molecular emission are linked to the disk property or process in question, review the deployed chemical probe(s), and discuss key results that have emerged or are expected in the near future.

5.1. Disk Gas Mass and Surface Density

The total disk mass and surface density set the planet formation potential of protoplanetary disks. Most of the disk mass and surface density consists of H_2, which cannot be directly observed; instead, a range of proxies have been developed, of which millimeter flux densities and CO isotopologue line fluxes are the most common (Andrews 2020, Miotello et al. 2022, and references therein). The utility of CO as a gas mass probe depends on how well known the CO abundance is in disks, which is fundamentally a chemical problem. The disk CO abundance structure has been modeled with different levels of sophistication, including CO freeze-out and photodissociation (e.g., Williams & Best 2014), self-shielding and isotope-selective photodissociation (Miotello et al. 2014), C and O isotopic fractionation chemistry (Miotello et al. 2016), and source-specific thermochemical models (van der Marel et al. 2015, 2016; Woitke et al. 2019; K. Zhang et al. 2021). When the CO model grids are compared with resolved or disk-integrated CO isotopologue fluxes and retrieved dust masses, the extracted gas-to-dust ratio is frequently one to two orders of magnitude below the typical ISM ratio of 100 (Miotello et al. 2017). A possible explanation is that models generally overestimate the CO abundance. This is supported by a small number of disk HD observations toward T Tauri disks, which reveal substantial CO depletion compared with the ISM (Bergin et al. 2013, McClure et al. 2016). Similar evidence for CO depletion is not observed for Herbig Ae disks, indicating that the depletion mechanism is sensitive to the specific disk conditions (Kama et al. 2020).

The observational evidence for CO depletion from the gas phase in T Tauri disks has triggered extensive modeling to understand its physicochemical cause(s). Some of the most commonly proposed scenarios (illustrated in **Figure 10**) include the following:

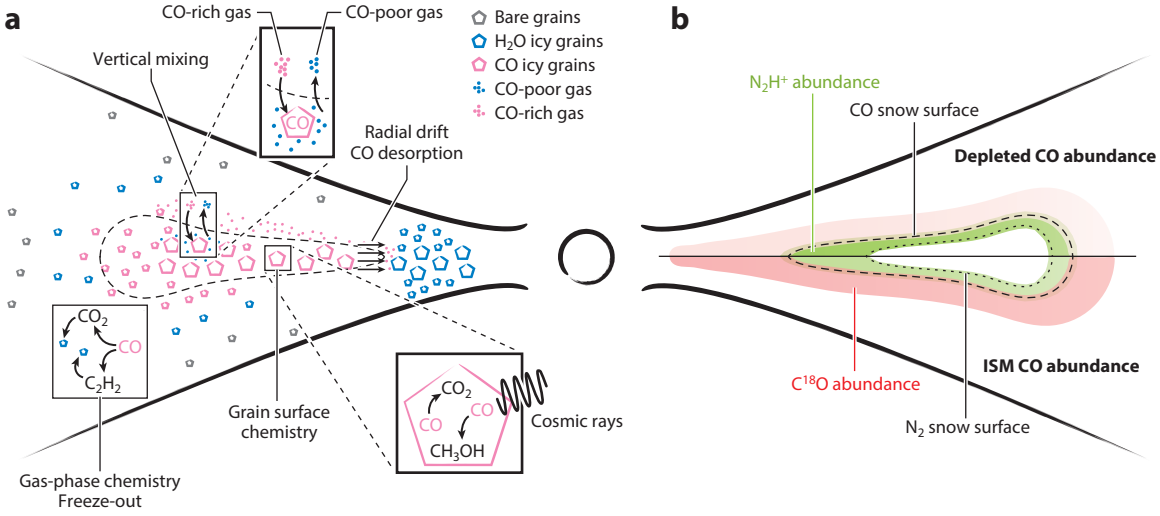

Figure 10

(*a*) Major physicochemical processes that reduce CO gas abundances in protoplanetary disks, including vertical mixing and sequestration of CO ice in the midplane, gas-phase chemistry and freeze-out, and grain surface chemistry. (*b*) $C^{18}O$ (*red*) and N_2H^+ (*green*) abundances (more intense color reflects higher abundance) for depleted and interstellar medium–like CO gas abundances.

1. Gas and dust vertical mixing, driven by large-scale motions or turbulence, can remove gaseous CO from the disk upper layers by freezing it onto large dust grains in the disk midplane (Kama et al. 2016, Powell et al. 2022). The same mechanism has been invoked to explain the low water abundance in the disk upper layers (Meijerink et al. 2009, Hogerheijde et al. 2011).
2. Gas-phase reactions can convert CO into less volatile species, such as CO_2 and small hydrocarbons (Aikawa & Herbst 1999, Yu et al. 2017), which subsequently freeze out onto dust grains.
3. Frozen-out CO may be transformed into molecules with higher binding energy, such as CO_2 or CH_3OH ice, through grain surface chemistry (Bosman et al. 2018, Schwarz et al. 2018).

Scenarios 1 and 3 should operate mainly outside the CO snowline, though radial diffusion may extend scenario 1 somewhat inward. The evidence that CO depletion is less severe in warm Herbig Ae disks where the CO snowline is further out supports these scenarios, and recent models by Krijt et al. (2020) and Van Clepper et al. (2022) show that both processes are needed to reproduce the derived low CO abundances of some T Tauri disks. These models also indicate that if dust radial drift is very effective, the CO abundance should be enhanced interior to the CO snowline, which has been observed toward some disks (e.g., K. Zhang et al. 2019). The precise CO depletion and enhancement levels for any given disk are, however, challenging to predict in this chemodynamical framework.

In light of the limitations of CO as a gas mass tracer, the community has explored complementary observational mass diagnostics, and N_2H^+ has emerged as a promising candidate. N_2H^+ should correlate with CO depletion (**Figure 10**), as a result of competition between N_2 and CO molecules for H_3^+, and N_2H^+ destruction by gas-phase CO. The combination of N_2H^+ and CO isotopologues should therefore probe both CO-rich and CO-poor gas and provide better mass estimates than CO-based ones (Anderson et al. 2022, Trapman et al. 2022). **Figure 11** shows that these chemical mass estimates are generally in good agreement with constraints from HD measurements when available. However, N_2H^+ fluxes also depend on ionizing radiation fluxes and the

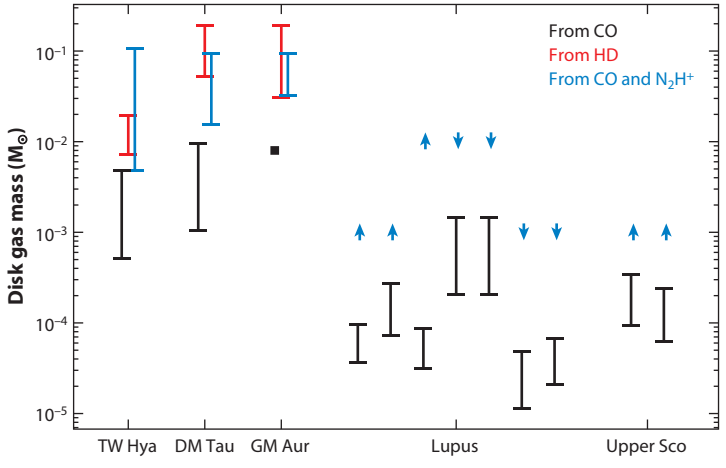

Figure 11

Comparison of total H_2 gas mass estimates using different molecular tracers: CO (*black*), HD (*red*), and N_2H^+ combined with CO (*blue*) (Thi et al. 2010; Miotello et al. 2016, 2017; Anderson et al. 2019, 2022; K. Zhang et al. 2019, 2021; Trapman et al. 2022).

cosmic-ray ionization rate, and an additional independent proxy of disk ionization (e.g., HCO^+) may be needed to consistently obtain accurate disk gas masses with this approach (van 't Hoff et al. 2017, Anderson et al. 2022). Other, complementary molecule-based methods to estimate gas masses are under development; these include the derivation of H_2 densities from excitation analyses of molecules not in LTE at a range of disk heights and radii (Teague & Loomis 2020). Finally, locations of snowlines may also be used to derive disk masses as a result of their dependence on pebble drift (Powell et al. 2019).

5.2. Disk Ionization

The ionization fraction of protoplanetary disks affects their dynamical and chemical evolution (see also discussion in Bergin et al. 2007). It regulates the coupling of the disk gas to magnetic field lines and, therefore, the efficacy of the magnetorotational instability in driving turbulence and disk evolution as well as in creating nonturbulent "dead zones" that are potentially favorable for planet formation (Gressel et al. 2012). Ionization also sets many chemical timescales. Ion–molecular reaction rates depend directly on ion abundances, and most grain surface and neutral–neutral gas-phase chemistry includes an ion recombination reaction to form the reactants. An example of the latter is the production of H atoms needed to form water on grain surfaces (Cleeves et al. 2014, Öberg & Bergin 2021).

Disk ionization studies typically have two goals: to determine the ionization fraction and to constrain the main source(s) of ionization (see Section 2.1). The ionization fraction is set by a balance between the ionization and recombination rates, both of which depend on the chemical composition of the disk (Semenov et al. 2004, Xu et al. 2019) as well as on the radiative transfer of the ionizing radiation. Due to the chemical stratification of protoplanetary disks, the main positive charge carrier varies between different disk regions (**Figure 12**), and the use of atomic and molecular ions as probes of ionization therefore depends on detailed models and observations of disk chemistry. Theoretically, atomic ions dominate near the directly irradiated, PDR-like disk surface, while molecular ions produced via protonation of abundant volatile species (H_2O, CO, N_2, NH_3) by H_3^+ dominate in the deeper layers. As shown in **Figure 12**, the thickness of the atomic ion layer and the region in which molecular ion is the major charge are both highly sensitive to the overall chemical state of a disk: In a disk depleted in C/H and O/H (see Section 4.2), the C^+ region is reduced in favor of H^+ and He^+, and the HCO^+ and H_3O^+ regions are reduced in

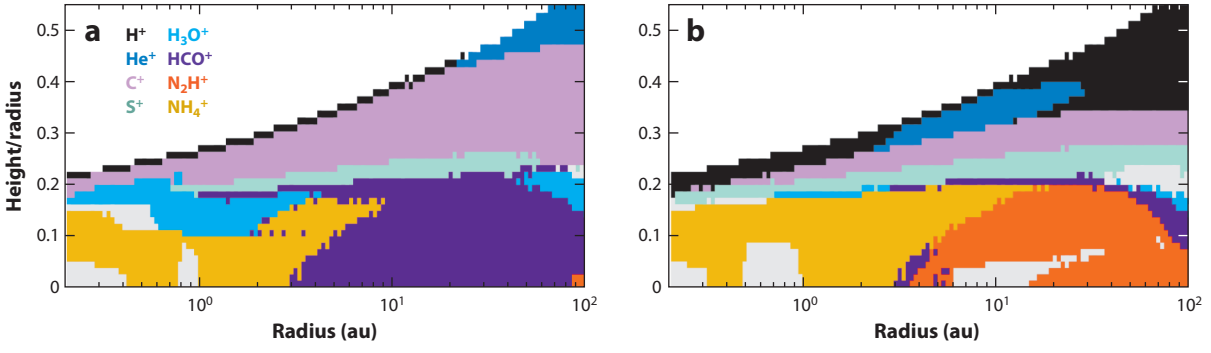

Figure 12

Dominant ion species across a T Tauri disk for models with (*a*) interstellar abundances of C and O and (*b*) initial C and O abundances depleted by 100-fold. Other minor species not listed in the legend are shown in gray. The models (Anderson et al. 2021, 2022) assume a stellar UV spectrum from a low-mass T Tauri star, a total X-ray luminosity of 10^{30} erg s^{-1}, and a cosmic-ray ionization rate of 10^{-18} s^{-1} per H_2 at the disk surface.

favor of the N-bearing molecular ions N_2H^+ and NH_4^+. Molecular ion abundances also depend on other elemental abundances, which act as electron donors (Ilgner & Nelson 2006). In addition to atomic and molecular ions, PAHs and grains can be significant charge carriers in the disk (e.g., Thi et al. 2019) (not shown in **Figure 12**).

Because of the complexity of the atomic and molecular ion structure of disks and the small number of studies focused on characterizing disk ionization, there is no consensus on the typical ionization level. On the basis of a combined analysis of HCO^+ and N_2H^+ emission in TW Hya, Cleeves et al. (2015b) found a low ionization level, which constrains the cosmic-ray ionization rate to be $\lesssim$0.01 times the interstellar value. By contrast, Aikawa et al. (2021) found relatively high ionization rates in both the warm molecular layer and the midplane of other disks, consistent with standard assumptions about X-ray ionization and relatively high cosmic-ray ionization rates. Finally, Seifert et al. (2021) found a gradient in the cosmic-ray ionization rate across the IM Lup disk. If this is a general feature, it may help explain some of the diverging results.

The relative importance of different sources of ionization should vary across disks (Cleeves et al. 2015b, Rab et al. 2018), between disks around different stars (Walsh et al. 2015), and in different radiation environments (Walsh et al. 2013). In theory, the contributions of different ionizing sources could be deduced from observations of ions in disks because different ionizing sources affect disk ion abundances in different disk regions. For example, Cleeves et al. (2015b) extracted a relatively limited contribution from cosmic-ray ionization and a larger-than-expected contribution from X-rays in one disk, suggesting a flaring X-ray stage. X-ray flares may also have a time-resolved impact on ionization, as observed by Cleeves et al. (2017). The full potential of ionization probes has yet to be realized, however, mainly because of a lack of comprehensive, spatially resolved molecular ion data sets on samples of disks.

5.3. Disk Temperature

Detailed disk temperature structures are necessary to correctly interpret molecular line observations, to model planet formation, and to predict the chemical evolution of disks (see also Sections 4.1 and 4.2). Molecular and atomic line observations constitute our best tools to constrain individual disk temperature structures as well as to benchmark disk models (e.g., Dartois et al. 2003, Piétu et al. 2007, Kamp et al. 2010, Calahan et al. 2021a). For spectrally well-resolved, optically thick lines, the peak brightness temperature (T_b) is a direct tracer of the local kinetic temperature, and spatially unresolved lines (including the CO ladder in the FIR) can be used to constrain disk gas temperatures by comparing observational data with radiative transfer models (e.g., Bruderer et al. 2012, van der Wiel et al. 2014). High spatial resolution observations of optically thick lines provide more direct constraints on the temperature profiles of the emitting layers (Dartois et al. 2003, K. Zhang et al. 2017, Pinte et al. 2018a). By combining optically thick lines emitting from different disk heights, which can be constrained observationally in mid-inclined disks (Section 3.6), one can reconstruct a 2D (R–z) map of the disk temperature. So far, this has mostly been done using CO isotopologues because of the high signal-to-noise ratios required by this method (Law et al. 2021b). However, future studies are also expected to make use of other molecules that emit from a larger range of disk layers because of either different chemistry or line excitation, which would enable a more complete temperature reconstruction (e.g., Huang et al. 2020).

For optically thin (or marginally optically thick) lines, single transitions cannot break the degeneracy between column density and excitation temperature. Instead, rotational excitation temperatures can be derived with molecular population diagrams using two or more transitions with well-characterized energy levels and transition probabilities. The high quality of ALMA data enables the construction of molecular population diagrams of numerous molecules, in several cases

also with spatially resolved data. Excitation temperatures have been derived for molecules such as HCN, H_2CO, CH_3OH, CH_3CN, CN, and c-C_3H_2 (e.g., Teague et al. 2015, Loomis et al. 2018a, Pegues et al. 2020, Teague & Loomis 2020, Facchini et al. 2021, Ilee et al. 2021, van der Marel et al. 2021). For marginally optically thick lines, it is possible to account for the line intensity saturation and correct for it (Goldsmith & Langer 1999). The critical density of most rotational transitions is less than 10^8 cm^{-3}, below the H/H_2 density where the lines originate and an LTE approximation is valid. Therefore, the excitation temperature directly traces the gas kinetic temperature and can be used as a gas thermometer when the emission location is known. Conversely, whenever the temperature structure is known through other means, the excitation temperature of molecules can be used to locate the vertical layer where the lines originate, anchoring disk chemistry models (Ilee et al. 2021).

In cases where molecular excitation temperatures are challenging to extract, including in the disk midplane, chemical structures can be used to constrain gas and dust temperatures. The most prominent examples are snowlines and snow surfaces (see Sections 4.1 and 3.6). Identification of snow surfaces via chemical markers (such as N_2H^+ for CO or $H^{13}CO^+$ for H_2O) uniquely associates a specific region of a disk with the range of sublimation temperatures obtained by laboratory experiments for that particular molecule (Fayolle et al. 2016, Qi et al. 2019, K. Zhang et al. 2021). Intensity ratios of some molecules have also been associated with specific gas temperatures and can be deployed as thermometers. The HNC/HCN ratio is an example of such a chemical thermometer, which works because of the temperature-dependent destruction of HNC (Graninger et al. 2015, Hacar et al. 2020, Long et al. 2021).

The deployment of these different temperature probes has confirmed general expectations for temperature structures (e.g., Dartois et al. 2003, Law et al. 2021b). Other observations have demonstrated the importance of gas heating in low-density disk environments (e.g., Fedele et al. 2016) and revealed unexpected thermal substructure, such as temperature inversions in outer disk regions, resulting in secondary snowlines of CO (Öberg et al. 2015a, Cleeves 2016, Dutrey et al. 2017, Facchini et al. 2017). An analogous thermal inversion can occur in the disk upper layers, where the dust and gas can sometimes thermally decouple at heights lower than those foreseen by thermochemical models that do not account for settling (e.g., Facchini et al. 2017). An open question in disk thermal structure modeling concerns the gas temperature in dust gaps and, hence, the chemical evolution in the vicinity of the planets that produce them. A higher penetration of energetic photons should increase both the gas and the dust temperatures (van der Marel et al. 2018, Alarcón et al. 2020, Rab et al. 2020), but efficient gas cooling may counteract this effect in severely dust-depleted gaps (Facchini et al. 2018b). Observational constraints on the gas temperature of dust gaps are inconclusive, but in at least two transition disk cavities the gas temperature is enhanced (Leemker et al. 2022).

5.4. Disk Dynamics and Planet Formation

Planet-forming disks are highly dynamical environments (Section 1.2; for recent reviews, see Armitage et al. 2020, Pinte et al. 2022), and many of these dynamical timescales are of the same order as (or shorter than) typical chemical timescales (e.g., Semenov & Wiebe 2011), complicating disk chemical modeling (Section 2.3). At the same time, chemistry can affect gas dynamics in disks through its impact on disk ionization and temperature (Sections 5.2 and 5.3), and a complete chemodynamical disk model would need to take this chemical feedback into account. The complex interplay between chemistry and dynamics is one of the major challenges for disk chemistry studies going forward. It is also a potential advantage, however, since it implies that chemical disk structures could be used as probes of disk dynamics and ongoing planet formation.

A set of proposed chemical probes of dynamics exploits the impact of radial advection of volatiles in the gas and/or ice form on inner disk molecular abundances (Section 1.2). Efficient inward radial drift of icy pebbles should increase the H_2O vapor in the inner disk and produce a substellar C/O ratio. This effect has been tentatively observed by Banzatti et al. (2020), who found an anticorrelation between inner disk H_2O line flux and pebble disk size, where a larger disk size implies less pebble drift (probably due to dust substructure). If, instead, water is sequestrated in the outer disk due to the efficient transformation of pebbles into boulders, the inner disk should be water poor and the C/O ratio superstellar. Najita et al. (2013) suggest that this process would explain an observed trend between the HCN/H_2O water ratio in the inner disk and disk mass. Upcoming JWST data may be able to distinguish between the two scenarios. Another possible probe of drift is the relative C/H ratios in the inner and outer disk regions (McClure 2019, Sturm et al. 2022). Disk models that include inward accretion flows have also noted large effects on the inner disk organic chemistry (Semenov & Wiebe 2011, Price et al. 2020), but these predicted effects have not yet been converted into an observational probe of inward gas transport.

Chemical disk structures can also be used to trace time-dependent changes in disk temperature and radiation structures. In an FU Ori outburst, a sudden increase in stellar luminosity and accretion rate moves the ice lines of molecules as H_2O and CH_3OH to large radii. The outwardly shifted snowlines remain for some time after the outburst and can therefore be used to infer an energetic past. This phenomenon has been observed in younger disks but not yet in mature protoplanetary disks (van 't Hoff et al. 2018b, Lee et al. 2019). Time-dependent changes in temperature and radiation can also be caused by disk warps. In warped disks, a misaligned inner disk can cast shadows onto the outer regions (Facchini et al. 2018a), and the resulting azimuthal gradient in the illumination pattern is expected to cause large-scale asymmetries in the intensity of molecular lines that are particularly sensitive to photochemistry (Young et al. 2021). Finally, theoretical models predict that heating from massive planets and UV excess caused by high accretion rates during the runaway phase could imprint the thermal and chemical structure of close-by gas as warm hot spots detectable with long ALMA integrations (Cleeves et al. 2015a). Such features have not yet been detected in the proximity of kinematically inferred planets (Pinte et al. 2018a, Casassus & Pérez 2019, Izquierdo et al. 2022) or directly detected planets (Facchini et al. 2021), but they constitute a potential unique probe of planet formation.

In addition to chemical probes, observations of molecular lines at high angular and spatial resolution can be used to directly constrain the gas dynamics of planet-forming disks. To date, almost all studies have made use of the brightest molecular lines, namely CO 2–1 and 3–2, without much regard for chemistry (e.g., Casassus & Pérez 2019, Teague et al. 2019, Izquierdo et al. 2021). However, there is real potential to further develop such probes in order to extract density and abundance gradients for different molecular species by mapping the velocity fields across the disk radial and vertical extent. In the meantime, such studies have revealed several kinematic structures relevant to the chemistry of planet formation. In particular, there are large-scale convective flows colocated with annular substructures in dust continuum (Teague et al. 2019, Yu et al. 2021). These meridional flows show that chemical abundances probed in disk molecular layers can access the planet-forming disk midplane and deliver chemically evolved gas to the proximity of growing protoplanets (Cridland et al. 2020).

6. LINKING DISK CHEMISTRY AND PLANET COMPOSITIONS

This review is largely motivated by a close connection between disk chemical structures and processes on the one hand and the outcome of planet formation on the other. In this final section, we review the links between disk chemistry and planet formation and discuss possible directions for future development.

To begin, snowline locations (Section 4.1) may affect the architectures of planetary systems. Snowlines of different volatiles are predicted to affect the grain coagulation rate, resulting in higher (or lower) rates of planet formation in the vicinity of snowline locations. In the Solar System, the presence of Jupiter at 5 au has long been associated with gas giant formation just outside the water snowline in the Solar Nebula (e.g., Stevenson & Lunine 1988). There is also evidence for a pileup of gas giant exoplanets around 2 au (Fernandes et al. 2019), which may coincide with the location of the water snowline during the relevant disk evolutionary stage. Better exoplanet statistics, as well as observations of snowline locations in samples of disks, are needed to establish such links between planet formation and snowline locations with confidence. Currently, CO and N_2 snowlines have been observed toward only a handful of disks, while H_2O snowline constraints are more indirect (and fewer), and no constraints exist for other major snowlines. This small number statistic is made worse by a clear bias toward atypical large and bright disks; therefore, it is difficult to extrapolate from existing disk snowline data to snowline locations in typical planet-forming disks. High-resolution ALMA data toward larger and less biased disk samples would resolve current uncertainties regarding CO and N_2 snowline locations, while the path forward for other snowline determinations is less clear and may require a combination of method development and new facilities.

Snowlines, or rather planet formation locations with respect to snowlines, should also affect planet compositions (Section 4.2). This idea has been used to constrain where in the Solar Nebula Jupiter and other planets formed on the basis of their compositions (e.g., Owen et al. 1999, Lodders 2004, Morbidelli et al. 2016, Bosman et al. 2019, Öberg & Wordsworth 2019), as well as to provide an interpretive framework for exoplanet compositions (Madhusudhan 2019) with a focus on atmospheric C/O ratios (Öberg et al. 2011b). Indeed, atmospheric elemental ratios have great potential to trace exoplanet histories, and while C/O ratios cannot be used on their own to assign an unambiguous planet formation location, C/O combined with C/N, C/H, and C/S should yield more informative constraints for gas giants (Öberg et al. 2011b, Piso et al. 2016, Hobbs et al. 2022), and other elemental ratios may be developed to trace the formation of smaller planets. The success of this method will require a more precise understanding of the distribution of elements in disks than is currently available, which will entail better models of the interactions between disk dynamics and molecule condensation and sublimation, as well as laboratory data on ice sublimation in different disk contexts (e.g., Fayolle et al. 2011, Potapov et al. 2018, Simon et al. 2019, Kruczkiewicz et al. 2021). In addition, if in situ chemistry is important for determining the major elemental carriers, then additional chemodynamical model development will be needed, along with laboratory experiments on the relevant chemical transformations.

Most research linking disk and planet composition has focused on the formation of giant planets and the elemental composition of their atmospheres, but in the near future the study of Earth analog atmospheres will become feasible. The atmospheres and hydrospheres of rocky planets are shaped by a range of processes, including outgassing of magma, the length of a magma ocean phase, plate tectonics (e.g., Lichtenberg et al. 2022 and references therein), and impacts of meteorites and comets. The last two connect the disk molecular inventories with rocky planet compositions; therefore, comprehensive data sets on the distribution of key organics in asteroid and comet-forming disk environments are needed to predict the prebiotic chemistry on young rocky planets. These will include both innovative observational constraints on disk icy reservoirs, such as those provided by Booth et al. (2021a), and models and laboratory data on the formation and transformation of organic molecules in disks. In the meantime, comparisons of organics in Solar System comets and a handful of protostellar and protoplanetary disks indicate that exoplanets assemble, at least sometimes, in a chemical environment similar to that of the Solar Nebula (Öberg et al. 2015b, 2021b; Drozdovskaya et al. 2019). In addition, constraining the distribution of life-enabling

elements like C, N, O, and P across disk solids will be crucial for determining their availability to terrestrial exoplanets (Bergin et al. 2015). For Earth analogs, it is also important to explore the links between refractory compositions of both inner disk solids and planet cores and mantles. The planet core composition is difficult to observe in regular planets, but it can be probed using data from extrasolar planetary bodies that have polluted white dwarf atmospheres (Jura & Young 2014).

Finally, isotopic ratios in gas and solids provide a tool to map the origins of cometary and planetary volatiles. So far, these ratios have been applied almost exclusively to the Solar System to constrain the origin of water on Earth and other planets, as well as in comets and asteroids (for reviews, see Ceccarelli et al. 2014, Altwegg et al. 2019). The first isotopic ratio in an exoplanet atmosphere was recently reported, potentially unlocking isotopic ratios as a complementary tool to elementary ratios when extracting a planet's formation history (Y. Zhang et al. 2021). The deployment of this method, however, requires a detailed understanding of the isotopic composition and fractionation chemistry of disks, which is currently incomplete. Additional observations, modeling, and experiments are needed to establish a comprehensive interpretative framework for planetary volatile isotopic compositions.

SUMMARY POINTS

1. Observations across the electromagnetic spectrum, from UV to radio wavelengths, are needed to characterize disk solid and gas compositions at all radii relevant to planet formation.
2. Disk chemical models, anchored in astrochemical computations and laboratory experiments, are essential to estimate the complete chemical compositions of disks and how they evolve over time.
3. Disk gas and solid elemental compositions often deviate from those of their host stars, which has a direct impact both on the disk organic chemistry and on the elemental and chemical makeup of planets.
4. The disk chemical structure and evolution are set by an interplay between chemical inheritance and a rich in situ chemistry. Accounting for both is especially important when considering the major carriers of the volatile elements and the organic inventory at different disk radii.
5. Multiple lines of evidence support substantial volatile transport and mixing in disks, which chemically connect inner and outer disks as well as disk midplanes and atmospheres.
6. Disk chemistry is closely intertwined with disk temperature and radiation structures, as well as with disk dynamics, illustrating the great potential of molecules as probes of nonchemical disk processes.

FUTURE ISSUES

1. During the past decade, ALMA disk chemistry observations have focused mostly on a small and highly biased sample of disks. Statistical samples of outer disk chemical compositions are needed to constrain the chemistry of "typical" planet formation and to link disk and exoplanet compositions.

2. Icy grains constitute the major reservoir of O, C, S, and P in disks. IR observations, informed by laboratory experiments, offer a great opportunity to characterize their compositions and determine whether they are inherited intact from the ISM or reformed in the disk.
3. Establishing clear chemodynamical links between different disk regions will require both the realization of new observational probes and further development of 2D (and eventually 3D) models that combine comprehensive chemical networks with a range of gas and dust dynamics and grain evolution.
4. The gas and solid compositions that are most relevant for terrestrial planet formation are currently not well constrained outside the Solar System. This limitation should be addressed by spectroscopic observations at the relevant scales and with models that connect the compositions of observable disk layers with the planet-forming midplane.
5. Several outstanding questions in disk chemistry studies, including the locations of key snowlines, the distribution of water, and the organic inventory across most of the planet-forming disk, may only be fully addressed by new observatories that provide access to the FIR as well as higher sensitivity at (sub)millimeter and radio wavelengths.

DISCLOSURE STATEMENT

The authors are not aware of any affiliations, memberships, funding, or financial holdings that might be perceived as affecting the objectivity of this review.

ACKNOWLEDGMENTS

We are grateful to Yuri Aikawa, Jennifer Bergner, Ewine van Dishoeck, Inga Kamp, Joan Najita, Colette Salyk, and Dmitry Semenov for insightful comments on the manuscript. We thank Anne Dutrey, Chunhua Qi, Kamber Schwarz, Hideko Nomura, and Charles Law for sharing data that have been used in this review. The writing of this review was supported by the Simons Foundation (grant 686302 and award 321183FY19 to K.I.Ö.) and the National Science Foundation (Astronomy and Astrophysics Research Grant 1907653 to K.I.Ö.). D.E.A. acknowledges support from a Virginia Initiative on Cosmic Origins Postdoctoral Fellowship and a Carnegie Postdoctoral Fellowship. S.F. is funded by the European Union under the European Union's Horizon Europe Research & Innovation Programme 101076613 (UNVEIL). Views and opinions expressed are however those of the author(s) only and do not necessarily reflect those of the European Union or the European Research Council. Neither the European Union nor the granting authority can be held responsible for them.

LITERATURE CITED

Acke B, van den Ancker ME, Dullemond CP, van Boekel R, Waters LBFM. 2004. *Astron. Astrophys.* 422:621–26
Ádámkovics M, Glassgold AE, Najita JR. 2014. *Astrophys. J.* 786(2):135
Agúndez M, Cernicharo J, Goicoechea JR. 2008. *Astron. Astrophys.* 483(3):831–37
Agúndez M, Roueff E, Le Petit F, Le Bourlot J. 2018. *Astron. Astrophys.* 616:A19
Aikawa Y, Cataldi G, Yamato Y, et al. 2021. *Astrophys. J. Suppl.* 257(1):13
Aikawa Y, Furuya K, Hincelin U, Herbst E. 2018. *Astrophys. J.* 855(2):119
Aikawa Y, Herbst E. 1999. *Astron. Astrophys.* 351:233–46
Aikawa Y, Herbst E. 2001. *Astron. Astrophys.* 371:1107–17

Aikawa Y, Kamuro D, Sakon I, et al. 2012. *Astron. Astrophys.* 538:A57
Aikawa Y, Miyama SM, Nakano T, Umebayashi T. 1996. *Astrophys. J.* 467:684–97
Aikawa Y, Momose M, Thi W, et al. 2003. *Publ. Astron. Soc. Jpn.* 55:11–15
Aikawa Y, Okuzumi S, Pontoppidan K. 2022. arXiv:2212.14529 [astro-ph.EP]
Aikawa Y, van Zadelhoff GJ, van Dishoeck EF, Herbst E. 2002. *Astron. Astrophys.* 386:622–32
Akimkin V, Zhukovska S, Wiebe D, et al. 2013. *Astrophys. J.* 766:8
Alarcón F, Teague R, Zhang K, Bergin EA, Barraza-Alfaro M. 2020. *Astrophys. J.* 905(1):68
Altwegg K, Balsiger H, Fuselier SA. 2019. *Annu. Rev. Astron. Astrophys.* 57:113–55
Altwegg K, Balsiger H, Hänni N, et al. 2020. *Nat. Astron.* 4:533–40
Anderson DE, Blake GA, Bergin EA, et al. 2019. *Astrophys. J.* 881(2):127
Anderson DE, Blake GA, Cleeves LI, et al. 2021. *Astrophys. J.* 909(1):55
Anderson DE, Cleeves LI, Blake GA, et al. 2022. *Astrophys. J.* 927(2):229
Andrews SM. 2015. *Publ. Astron. Soc. Pac.* 127(956):961–93
Andrews SM. 2020. *Annu. Rev. Astron. Astrophys.* 58:483–528
Andrews SM, Huang J, Pérez LM, et al. 2018. *Astrophys. J. Lett.* 869(2):L41
Ansdell M, Williams JP, van der Marel N, et al. 2016. *Astrophys. J.* 828(1):46
Antonellini S, Kamp I, Lahuis F, et al. 2016. *Astron. Astrophys.* 585:A61
Ardila DR, Herczeg GJ, Gregory SG, et al. 2013. *Astrophys. J. Suppl.* 207(1):1
Armitage PJ, Bae J, Benisty M, et al. (Disk Dyn. Collab.). 2020. arXiv:2009.04345 [astro-ph.EP]
Armitage PJ, Livio M, Pringle JE. 2001. *Mon. Not. R. Astron. Soc.* 324(3):705–11
Arulanantham N, France K, Hoadley K, et al. 2021. *Astron. J.* 162(5):185
Bai XN, Stone JM. 2013. *Astrophys. J.* 769(1):76
Ballering NP, Cleeves LI, Anderson DE. 2021. *Astrophys. J.* 920(2):115
Banzatti A, Meyer MR, Bruderer S, et al. 2012. *Astrophys. J.* 745(1):90
Banzatti A, Pascucci I, Bosman AD, et al. 2020. *Astrophys. J.* 903(2):124
Banzatti A, Pinilla P, Ricci L, et al. 2015. *Astrophys. J. Lett.* 815:L15
Banzatti A, Pontoppidan KM, Pérez Chávez J, et al. 2022. arXiv:2209.08216 [astro-ph.EP]
Bar-Nun A, Herman G, Laufer D, Rappaport ML. 1985. *Icarus* 63:317–32
Barenfeld SA, Carpenter JM, Ricci L, Isella A. 2016. *Astrophys. J.* 827(2):142
Bergin EA, Aikawa Y, Blake GA, van Dishoeck EF. 2007. In *Protostars and Planets V*, ed. B Reipurth, D Jewitt, K Keil, pp. 751–66. Tucson: Univ. Ariz. Press
Bergin EA, Alexander C, Drozdovskaya M, Gounelle M, Pfalzner S. 2023. arXiv:2301.05212 [astro-ph.EP]
Bergin EA, Blake GA, Ciesla F, Hirschmann MM, Li J. 2015. *PNAS* 112:8965–70
Bergin EA, Cleeves LI, Gorti U, et al. 2013. *Nature* 493:644–46
Bergin EA, Langer WD, Goldsmith PF. 1995. *Astrophys. J.* 441:222–43
Bergner JB, Ciesla F. 2021. *Astrophys. J.* 919(1):45
Bergner JB, Guzmán VG, Öberg KI, Loomis RA, Pegues J. 2018. *Astrophys. J.* 857:69
Bergner JB, Öberg KI, Bergin EA, et al. 2019. *Astrophys. J.* 876(1):25
Bergner JB, Öberg KI, Bergin EA, et al. 2020. *Astrophys. J.* 898(2):97
Bergner JB, Öberg KI, Guzmán VV, et al. 2021. *Astrophys. J. Suppl.* 257(1):11
Bernstein MP, Dworkin JP, Sandford SA, Cooper GW, Allamandola LJ. 2002. *Nature* 416:401–3
Bethell TJ, Bergin EA. 2011. *Astrophys. J.* 739:78
Bjerkeli P, Jørgensen JK, Bergin EA, et al. 2016. *Astron. Astrophys.* 595:A39
Blevins SM, Pontoppidan KM, Banzatti A, et al. 2016. *Astrophys. J.* 818(1):22
Bockelée-Morvan D, Calmonte U, Charnley S, et al. 2015. *Space Sci. Rev.* 197(1–4):47–83
Boogert ACA, Gerakines PA, Whittet DCB. 2015. *Annu. Rev. Astron. Astrophys.* 53:541–81
Booth AS, van der Marel N, Leemker M, van Dishoeck EF, Ohashi S. 2021a. *Astron. Astrophys.* 651:L6
Booth AS, Walsh C, Ilee JD, et al. 2019. *Astrophys. J. Lett.* 882(2):L31
Booth AS, Walsh C, Terwisscha van Scheltinga J, et al. 2021b. *Nat. Astron.* 5:684–90
Booth RA, Ilee JD. 2019. *Mon. Not. R. Astron. Soc.* 487(3):3998–4011
Bosman AD, Alarcón F, Bergin EA, et al. 2021a. *Astrophys. J. Suppl.* 257(1):7
Bosman AD, Alarcón F, Zhang K, Bergin EA. 2021b. *Astrophys. J.* 910(1):3

Bosman AD, Bergin EA, Loomis RA, et al. 2021c. *Astrophys. J. Suppl.* 257(1):15
Bosman AD, Bruderer S, van Dishoeck EF. 2017. *Astron. Astrophys.* 601:A36
Bosman AD, Cridland AJ, Miguel Y. 2019. *Astron. Astrophys.* 632:L11
Bosman AD, Walsh C, van Dishoeck EF. 2018. *Astron. Astrophys.* 618:A182
Bouwman J, Henning T, Hillenbrand LA, et al. 2008. *Astrophys. J.* 683(1):479–98
Brinch C, Hogerheijde MR. 2010. *Astron. Astrophys.* 523:A25
Brittain SD, Simon T, Najita JR, Rettig TW. 2007. *Astrophys. J.* 659(1):685–704
Bruderer S. 2013. *Astron. Astrophys.* 559:A46
Bruderer S, Harsono D, van Dishoeck EF. 2015. *Astron. Astrophys.* 575:A94
Bruderer S, van Dishoeck EF, Doty SD, Herczeg GJ. 2012. *Astron. Astrophys.* 541:A91
Brunken NGC, Booth AS, Leemker M, et al. 2022. *Astron. Astrophys.* 659:A29
Calahan JK, Bergin EA, Zhang K, et al. 2021a. *Astrophys. J. Suppl.* 257(1):17
Calahan JK, Bergin EA, Zhang K, et al. 2021b. *Astrophys. J.* 908(1):8
Canta A, Teague R, Le Gal R, Öberg KI. 2021. *Astrophys. J.* 922(1):62
Carr JS, Najita JR. 2008. *Science* 319:1504–6
Carr JS, Najita JR. 2011. *Astrophys. J.* 733(2):102
Carr JS, Najita JR, Salyk C. 2018. *Res. Notes Am. Astron. Soc.* 2(3):169
Casassus S, Christiaens V, Cárcamo M, et al. 2021. *Mon. Not. R. Astron. Soc.* 507(3):3789–809
Casassus S, Pérez S. 2019. *Astrophys. J. Lett.* 883(2):L41
Cataldi G, Yamato Y, Aikawa Y, et al. 2021. *Astrophys. J. Suppl.* 257(1):10
Cazzoletti P, van Dishoeck EF, Visser R, Facchini S, Bruderer S. 2018. *Astron. Astrophys.* 609:A93
Ceccarelli C, Caselli P, Bockelée-Morvan D, et al. 2014. In *Protostars and Planets VI*, ed. H Beuther, RS Klessen, CP Dullemond, T Henning, pp. 859–82. Baltimore, MD: Johns Hopkins Univ. Press
Chapillon E, Dutrey A, Guilloteau S, et al. 2012. *Astrophys. J.* 756:58
Chiang E, Youdin AN. 2010. *Annu. Rev. Earth Planet. Sci.* 38:493–522
Chiang EI, Goldreich P. 1997. *Astrophys. J.* 490:368–76
Chuang KJ, Fedoseev G, Qasim D, et al. 2017. *Mon. Not. R. Astron. Soc.* 467(3):2552–65
Ciesla FJ, Cuzzi JN. 2006. *Icarus* 181:178–204
Ciesla FJ, Sandford SA. 2012. *Science* 336:452–54
Cieza LA, Casassus S, Tobin J, et al. 2016. *Nature* 535:258–61
Cleeves LI. 2016. *Astrophys. J. Lett.* 816:L21
Cleeves LI, Bergin EA, Alexander CMO, et al. 2014. *Science* 345:1590–93
Cleeves LI, Bergin EA, Harries TJ. 2015a. *Astrophys. J.* 807:2
Cleeves LI, Bergin EA, Öberg KI, et al. 2017. *Astrophys. J. Lett.* 843(1):L3
Cleeves LI, Bergin EA, Qi C, Adams FC, Öberg KI. 2015b. *Astrophys. J.* 799:204
Cleeves LI, Öberg KI, Wilner DJ, et al. 2018. *Astrophys. J.* 865(2):155
Collings MP, Anderson MA, Chen R, et al. 2004. *Mon. Not. R. Astron. Soc.* 354:1133–40
Collings MP, Dever JW, Fraser HJ, McCoustra MRS. 2003. *Astrophys. Space Sci.* 285:633–59
Cridland AJ, van Dishoeck EF, Alessi M, Pudritz RE. 2020. *Astron. Astrophys.* 642:A229
Cuzzi JN, Zahnle KJ. 2004. *Astrophys. J.* 614(1):490–96
D'Alessio P, Calvet N, Hartmann L, Franco-Hernández R, Servín H. 2006. *Astrophys. J.* 638:314–35
D'Alessio P, Calvet N, Hartmann L, Lizano S, Cantó J. 1999. *Astrophys. J.* 527:893–909
Dartois E, Dutrey A, Guilloteau S. 2003. *Astron. Astrophys.* 399:773–87
Drake JJ, Testa P, Hartmann L. 2005. *Astrophys. J. Lett.* 627(2):L149–52
Drazkowska J, Bitsch B, Lambrechts M, et al. 2022. arXiv:2203.09759 [astro-ph.EP]
Drozdovskaya MN, van Dishoeck EF, Rubin M, Jørgensen JK, Altwegg K. 2019. *Mon. Not. R. Astron. Soc.* 490(1):50–79
Drozdovskaya MN, Walsh C, van Dishoeck EF, et al. 2016. *Mon. Not. R. Astron. Soc.* 462(1):977–93
Du F, Bergin EA. 2014. *Astrophys. J.* 792(1):2
Du F, Bergin EA, Hogerheijde MR. 2015. *Astrophys. J. Lett.* 807:L32
Dutrey A, Guilloteau S, Duvert G, et al. 1996. *Astron. Astrophys.* 309:493–504
Dutrey A, Guilloteau S, Piétu V, et al. 2008. *Astron. Astrophys.* 490:L15–18

Dutrey A, Guilloteau S, Piétu V, et al. 2017. *Astron. Astrophys.* 607:A130
Dutrey A, Henning T, Guilloteau S, et al. 2007. *Astron. Astrophys.* 464:615–23
Dutrey A, Semenov D, Chapillon E, et al. 2014. In *Protostars and Planets VI*, ed. H Beuther, RS Klessen, CP Dullemond, T Henning, pp. 317–38. Baltimore, MD: Johns Hopkins Univ. Press
Duval SE, Bosman AD, Bergin EA. 2022. *Astrophys. J. Lett.* 934(2):L25
Eistrup C, Henning T. 2022. *Astron. Astrophys.* 667:A160
Eistrup C, Walsh C, van Dishoeck EF. 2016. *Astron. Astrophys.* 595:A83
Endres CP, Schlemmer S, Schilke P, Stutzki J, Müller HSP. 2016. *J. Mol. Spectrosc.* 327:95–104
Facchini S, Birnstiel T, Bruderer S, van Dishoeck EF. 2017. *Astron. Astrophys.* 605:A16
Facchini S, Juhász A, Lodato G. 2018a. *Mon. Not. R. Astron. Soc.* 473(4):4459–75
Facchini S, Manara CF, Schneider PC, et al. 2016. *Astron. Astrophys.* 596:A38
Facchini S, Pinilla P, van Dishoeck EF, de Juan Ovelar M. 2018b. *Astron. Astrophys.* 612:A104
Facchini S, Teague R, Bae J, et al. 2021. *Astron. J.* 162(3):99
Faure M, Quirico E, Faure A, et al. 2015. *Icarus* 261:14–30
Fayolle EC, Balfe J, Loomis R, et al. 2016. *Astrophys. J. Lett.* 816:L28
Fayolle EC, Bertin M, Romanzin C, et al. 2011. *Astrophys. J. Lett.* 739:L36
Fedele D, Bruderer S, van Dishoeck EF, et al. 2013. *Astron. Astrophys.* 559:A77
Fedele D, Favre C. 2020. *Astron. Astrophys.* 638:A110
Fedele D, van Dishoeck EF, Kama M, Bruderer S, Hogerheijde MR. 2016. *Astron. Astrophys.* 591:A95
Fernandes RB, Mulders GD, Pascucci I, Mordasini C, Emsenhuber A. 2019. *Astrophys. J.* 874(1):81
France K, Schindhelm R, Herczeg GJ, et al. 2012. *Astrophys. J.* 756(2):171
Fuchs GW, Cuppen HM, Ioppolo S, et al. 2009. *Astron. Astrophys.* 505:629–39
Fuente A, Cernicharo J, Agúndez M, et al. 2010. *Astron. Astrophys.* 524:A19
Furuya K, Aikawa Y. 2014. *Astrophys. J.* 790:97
Furuya K, Tsukagoshi T, Qi C, et al. 2022. *Astrophys. J.* 926(2):148
Gavino S, Dutrey A, Wakelam V, et al. 2021. *Astron. Astrophys.* 654:A65
Geers VC, Augereau JC, Pontoppidan KM, et al. 2006. *Astron. Astrophys.* 459(2):545–56
Gibb EL, Van Brunt KA, Brittain SD, Rettig TW. 2007. *Astrophys. J.* 660(2):1572–79
Glassgold AE, Meijerink R, Najita JR. 2009. *Astrophys. J.* 701(1):142–53
Glassgold AE, Najita J, Igea J. 2004. *Astrophys. J.* 615(2):972–90
Goldsmith PF, Langer WD. 1999. *Astrophys. J.* 517:209–25
Gordon IE, Rothman LS, Hargreaves RJ, et al. 2022. *J. Quant. Spectrosc. Radiat. Transf.* 277:107949
Graninger D, Öberg KI, Qi C, Kastner J. 2015. *Astrophys. J. Lett.* 807:L15
Grant SL, van Dishoeck EF, Tabone B, et al. 2022. arXiv:2212.08047 [astro-ph.SR]
Gressel O, Nelson RP, Turner NJ. 2012. *Mon. Not. R. Astron. Soc.* 422(2):1140–59
Guilloteau S, Di Folco E, Dutrey A, et al. 2013. *Astron. Astrophys.* 549:A92
Guilloteau S, Reboussin L, Dutrey A, et al. 2016. *Astron. Astrophys.* 592:A124
Gundlach B, Blum J. 2015. *Astrophys. J.* 798:34
Günther HM, Birnstiel T, Huenemoerder DP, et al. 2018. *Astron. J.* 156(2):56
Guzmán VV, Bergner JB, Law CJ, et al. 2021. *Astrophys. J. Suppl.* 257(1):6
Guzmán VV, Huang J, Andrews SM, et al. 2018. *Astrophys. J. Lett.* 869(2):L48
Guzmán VV, Öberg KI, Huang J, Loomis R, Qi C. 2017. *Astrophys. J.* 836:30
Hacar A, Bosman AD, van Dishoeck EF. 2020. *Astron. Astrophys.* 635:A4
Hartmann L, Calvet N, Gullbring E, D'Alessio P. 1998. *Astrophys. J.* 495:385–400
Heays AN, Visser R, Gredel R, et al. 2014. *Astron. Astrophys.* 562:A61
Henning T, Semenov D. 2013. *Chem. Rev.* 113:9016–42
Henning T, Semenov D, Guilloteau S, et al. 2010. *Astrophys. J.* 714(2):1511–20
Hersant F, Wakelam V, Dutrey A, Guilloteau S, Herbst E. 2009. *Astron. Astrophys.* 493:L49–52
Hidaka H, Watanabe N, Shiraki T, Nagaoka A, Kouchi A. 2004. *Astrophys. J.* 614(2):1124–31
Hily-Blant P, Magalhaes V, Kastner J, et al. 2017. *Astron. Astrophys.* 603:L6
Hily-Blant P, Magalhaes de Souza V, Kastner J, Forveille T. 2019. *Astron. Astrophys.* 632:L12
Hobbs R, Shorttle O, Madhusudhan N. 2022. *Mon. Not. R. Astron. Soc.* 516(1):1032–46

Hogerheijde MR, Bergin EA, Brinch C, et al. 2011. *Science* 334:338–40
Hogerheijde MR, van der Tak FFS. 2000. *Astron. Astrophys.* 362:697–710
Honda M, Inoue AK, Fukagawa M, et al. 2009. *Astrophys. J. Lett.* 690(2):L110–13
Huang J, Andrews SM, Cleeves LI, et al. 2018a. *Astrophys. J.* 852:122
Huang J, Andrews SM, Dullemond CP, et al. 2018b. *Astrophys. J. Lett.* 869(2):L42
Huang J, Andrews SM, Dullemond CP, et al. 2020. *Astrophys. J.* 891(1):48
Huang J, Bergin EA, Öberg KI, et al. 2021. *Astrophys. J. Suppl.* 257(1):19
Huang J, Öberg KI. 2015. *Astrophys. J. Lett.* 809(2):L26
Huang J, Öberg KI, Qi C, et al. 2017. *Astrophys. J.* 835:231
Ilee JD, Walsh C, Booth AS, et al. 2021. *Astrophys. J. Suppl.* 257(1):9
Ilgner M, Henning T, Markwick AJ, Millar TJ. 2004. *Astron. Astrophys.* 415:643–59
Ilgner M, Nelson RP. 2006. *Astron. Astrophys.* 445(1):205–22
Ioppolo S, Fedoseev G, Chuang KJ, et al. 2021. *Nat. Astron.* 5:197–205
Izquierdo AF, Facchini S, Rosotti GP, van Dishoeck EF, Testi L. 2022. *Astrophys. J.* 928(1):2
Izquierdo AF, Testi L, Facchini S, Rosotti GP, van Dishoeck EF. 2021. *Astron. Astrophys.* 650:A179
Jiang H, Zhu W, Ormel CW. 2022. *Astrophys. J. Lett.* 924(2):L31
Jonkheid B, Faas FGA, van Zadelhoff G, van Dishoeck EF. 2004. *Astron. Astrophys.* 428:511–21
Jørgensen JK, Belloche A, Garrod RT. 2020. *Annu. Rev. Astron. Astrophys.* 58:727–78
Jura M, Young ED. 2014. *Annu. Rev. Earth Planet. Sci.* 42:45–67
Kama M, Bruderer S, Carney M, et al. 2016. *Astron. Astrophys.* 588:A108
Kama M, Shorttle O, Jermyn AS, et al. 2019. *Astrophys. J.* 885(2):114
Kama M, Trapman L, Fedele D, et al. 2020. *Astron. Astrophys.* 634:A88
Kamp I, Dullemond CP. 2004. *Astrophys. J.* 615(2):991–99
Kamp I, Thi WF, Meeus G, et al. 2013. *Astron. Astrophys.* 559:A24
Kamp I, Thi WF, Woitke P, et al. 2017. *Astron. Astrophys.* 607:A41
Kamp I, Tilling I, Woitke P, Thi WF, Hogerheijde M. 2010. *Astron. Astrophys.* 510:A18
Kastner JH, Hily-Blant P, Rodriguez DR, Punzi K, Forveille T. 2014. *Astrophys. J.* 793:55
Kastner JH, Zuckerman B, Weintraub DA, Forveille T. 1997. *Science* 277:67–71
Kress ME, Tielens AGGM, Frenklach M. 2010. *Adv. Space Res.* 46(1):44–49
Krijt S, Bosman AD, Zhang K, et al. 2020. *Astrophys. J.* 899(2):134
Krijt S, Ciesla FJ, Bergin EA. 2016. *Astrophys. J.* 833(2):285
Krijt S, Schwarz KR, Bergin EA, Ciesla FJ. 2018. *Astrophys. J.* 864(1):78
Kruczkiewicz F, Vitorino J, Congiu E, Theulé P, Dulieu F. 2021. *Astron. Astrophys.* 652:A29
Lahuis F, van Dishoeck EF, Blake GA, et al. 2007. *Astrophys. J.* 665(1):492–511
Law CJ, Crystian S, Teague R, et al. 2022. *Astrophys. J.* 932(2):114
Law CJ, Loomis RA, Teague R, et al. 2021a. *Astrophys. J. Suppl.* 257(1):3
Law CJ, Teague R, Loomis RA, et al. 2021b. *Astrophys. J. Suppl.* 257(1):4
Le Gal R, Brady MT, Öberg KI, Roueff E, Le Petit F. 2019a. *Astrophys. J.* 886(2):86
Le Gal R, Öberg KI, Loomis RA, Pegues J, Bergner JB. 2019b. *Astrophys. J.* 876(1):72
Le Gal R, Öberg KI, Teague R, et al. 2021. *Astrophys. J. Suppl.* 257(1):12
Lee JE, Lee S, Baek G, et al. 2019. *Nat. Astron.* 3:314–19
Leemker M, Booth AS, van Dishoeck EF, et al. 2022. *Astron. Astrophys.* 663:A23
Leemker M, van 't Hoff MLR, Trapman L, et al. 2021. *Astron. Astrophys.* 646:A3
Lichtenberg T, Schaefer LK, Nakajima M, Fischer RA. 2022. arXiv:2203.10023 [astro-ph.EP]
Lodders K. 2003. *Astrophys. J.* 591:1220–47
Lodders K. 2004. *Astrophys. J.* 611:587–97
Long F, Bosman AD, Cazzoletti P, et al. 2021. *Astron. Astrophys.* 647:A118
Long F, Herczeg GJ, Pascucci I, et al. 2017. *Astrophys. J.* 844(2):99
Long F, Pinilla P, Herczeg GJ, et al. 2018. *Astrophys. J.* 869(1):17
Loomis RA, Cleeves LI, Öberg KI, et al. 2018a. *Astrophys. J.* 859:131
Loomis RA, Öberg KI, Andrews SM, et al. 2018b. *Astron. J.* 155:182
Loomis RA, Öberg KI, Andrews SM, et al. 2020. *Astrophys. J.* 893(2):101

Lunine JI, Stevenson DJ. 1985. *Astrophys. J. Suppl.* 58:493–531
Lynden-Bell D, Pringle JE. 1974. *Mon. Not. R. Astron. Soc.* 168:603–37
Lyons JR, Young ED. 2005. *ASP Conf. Proc.* 341:193–211
Madhusudhan N. 2019. *Annu. Rev. Astron. Astrophys.* 57:617–63
Mandell AM, Bast J, van Dishoeck EF, et al. 2012. *Astrophys. J.* 747(2):92
McClure MK. 2019. *Astron. Astrophys.* 632:A32
McClure MK, Bergin EA, Cleeves LI, et al. 2016. *Astrophys. J.* 831(2):167
McElroy D, Walsh C, Markwick AJ, et al. 2013. *Astron. Astrophys.* 550:A36
McGuire BA. 2022. *Astrophys. J. Suppl.* 259(2):30
Meeus G, Montesinos B, Mendigutía I, et al. 2012. *Astron. Astrophys.* 544:A78
Meeus G, Salyk C, Bruderer S, et al. 2013. *Astron. Astrophys.* 559:A84
Meijerink R, Pontoppidan KM, Blake GA, Poelman DR, Dullemond CP. 2009. *Astrophys. J.* 704:1471–81
Min M, Bouwman J, Dominik C, et al. 2016. *Astron. Astrophys.* 593:A11
Miotello A, Bruderer S, van Dishoeck EF. 2014. *Astron. Astrophys.* 572:A96
Miotello A, Facchini S, van Dishoeck EF, et al. 2019. *Astron. Astrophys.* 631:A69
Miotello A, Kamp I, Birnstiel T, Cleeves LI, Kataoka A. 2022. arXiv:2203.09818 [astro-ph.EP]
Miotello A, van Dishoeck EF, Kama M, Bruderer S. 2016. *Astron. Astrophys.* 594:A85
Miotello A, van Dishoeck EF, Williams JP, et al. 2017. *Astron. Astrophys.* 599:A113
Molyarova T, Akimkin V, Semenov D, et al. 2018. *Astrophys. J.* 866(1):46
Morbidelli A, Bitsch B, Crida A, et al. 2016. *Icarus* 267:368–76
Muñoz Caro GM, Meierhenrich UJ, Schutte WA, et al. 2002. *Nature* 416:403–6
Müller HSP, Schlöder F, Stutzki J, Winnewisser G. 2005. *J. Mol. Struct.* 742:215–27
Müller HSP, Thorwirth S, Roth DA, Winnewisser G. 2001. *Astron. Astrophys.* 370:L49–52
Mumma MJ, Charnley SB. 2011. *Annu. Rev. Astron. Astrophys.* 49:471–524
Najita JR, Ádámkovics M. 2017. *Astrophys. J.* 847(1):6
Najita JR, Ádámkovics M, Glassgold AE. 2011. *Astrophys. J.* 743(2):147
Najita JR, Carr JS, Brittain SD, et al. 2021. *Astrophys. J.* 908(2):171
Najita JR, Carr JS, Mathieu RD. 2003. *Astrophys. J.* 589(2):931–52
Najita JR, Carr JS, Pontoppidan KM, et al. 2013. *Astrophys. J.* 766:134
Najita JR, Carr JS, Salyk C, et al. 2018. *Astrophys. J.* 862(2):122
Najita JR, Carr JS, Strom SE, et al. 2010. *Astrophys. J.* 712(1):274–86
Natta A, Testi L, Calvet N, et al. 2007. In *Protostars and Planets V*, ed. B Reipurth, D Jewitt, K Keil, pp. 767–81. Tucson: Univ. Ariz. Press
Nomura H, Aikawa Y, Nakagawa Y, Millar TJ. 2009. *Astron. Astrophys.* 495(1):183–88
Nomura H, Aikawa Y, Tsujimoto M, Nakagawa Y, Millar TJ. 2007. *Astrophys. J.* 661:334–53
Nomura H, Tsukagoshi T, Kawabe R, et al. 2021. *Astrophys. J.* 914(2):113
Öberg KI, Bergin EA. 2021. *Phys. Rep.* 893:1–48
Öberg KI, Boogert ACA, Pontoppidan KM, et al. 2011a. *Astrophys. J.* 740:109
Öberg KI, Cleeves LI, Bergner JB, et al. 2021a. *Astron. J.* 161(1):38
Öberg KI, Furuya K, Loomis R, et al. 2015a. *Astrophys. J.* 810:112
Öberg KI, Guzmán VV, Furuya K, et al. 2015b. *Nature* 520:198–201
Öberg KI, Guzmán VV, Walsh C, et al. 2021b. *Astrophys. J. Suppl.* 257(1):1
Öberg KI, Murray-Clay R, Bergin EA. 2011b. *Astrophys. J. Lett.* 743:L16
Öberg KI, Qi C, Fogel JKJ, et al. 2010. *Astrophys. J.* 720:480–93
Öberg KI, Qi C, Fogel JKJ, et al. 2011c. *Astrophys. J.* 734:98
Öberg KI, Wordsworth R. 2019. *Astron. J.* 158(5):194
Okuzumi S, Tazaki R. 2019. *Astrophys. J.* 878(2):132
Owen T, Mahaffy P, Niemann HB, et al. 1999. *Nature* 402:269–70
Paneque-Carreño T, Miotello A, van Dishoeck EF, et al. 2022. arXiv:2207.08827 [astro-ph.EP]
Pascucci I, Apai D, Luhman K, et al. 2009. *Astrophys. J.* 696:143–59
Pascucci I, Cabrit S, Edwards S, et al. 2022. arXiv:2203.10068 [astro-ph.SR]
Pascucci I, Herczeg G, Carr JS, Bruderer S. 2013. *Astrophys. J.* 779(2):178

Pegues J, Öberg KI, Bergner JB, et al. 2020. *Astrophys. J.* 890(2):142
Pegues J, Öberg KI, Bergner JB, et al. 2021. *Astrophys. J.* 911(2):150
Phuong NT, Chapillon E, Majumdar L, et al. 2018. *Astron. Astrophys.* 616:L5
Phuong NT, Dutrey A, Chapillon E, et al. 2021. *Astron. Astrophys.* 653:L5
Pickett HM, Poynter RL, Cohen EA, et al. 1998. *J. Quant. Spectrosc. Radiat. Transf.* 60:883–90
Piétu V, Dutrey A, Guilloteau S. 2007. *Astron. Astrophys.* 467:163–78
Pinte C, Ménard F, Duchêne G, Bastien P. 2006. *Astron. Astrophys.* 459(3):797–804
Pinte C, Ménard F, Duchêne G, et al. 2018a. *Astron. Astrophys.* 609:A47
Pinte C, Price DJ, Ménard F, et al. 2018b. *Astrophys. J. Lett.* 860(1):L13
Pinte C, Teague R, Flaherty K, et al. 2022. arXiv:2203.09528 [astro-ph.EP]
Pirovano LM, Fedele D, van Dishoeck EF, et al. 2022. *Astron. Astrophys.* 665:A45
Piso AMA, Öberg KI, Birnstiel T, Murray-Clay RA. 2015. *Astrophys. J.* 815:109
Piso AMA, Pegues J, Öberg KI. 2016. *Astrophys. J.* 833(2):203
Podio L, Garufi A, Codella C, et al. 2020. *Astron. Astrophys.* 642:L7
Pontoppidan KM, Blake GA, Smette A. 2011. *Astrophys. J.* 733(2):84
Pontoppidan KM, Blake GA, van Dishoeck EF, et al. 2008. *Astrophys. J.* 684:1323–29
Pontoppidan KM, Dullemond CP, van Dishoeck EF, et al. 2005. *Astrophys. J.* 622:463–81
Pontoppidan KM, Meijerink R, Dullemond CP, Blake GA. 2009. *Astrophys. J.* 704(2):1482–94
Pontoppidan KM, Salyk C, Banzatti A, et al. 2019. *Astrophys. J.* 874(1):92
Pontoppidan KM, Salyk C, Bergin EA, et al. 2014. In *Protostars and Planets VI*, ed. H Beuther, RS Klessen, CP Dullemond, T Henning, pp. 363–86. Baltimore, MD: Johns Hopkins Univ. Press
Pontoppidan KM, Salyk C, Blake GA, et al. 2010. *Astrophys. J.* 720:887–903
Potapov A, Jäger C, Henning T. 2018. *Astrophys. J.* 865(1):58
Powell D, Gao P, Murray-Clay R, Zhang X. 2022. *Nat. Astron.* 6:1147–55
Powell D, Murray-Clay R, Pérez LM, Schlichting HE, Rosenthal M. 2019. *Astrophys. J.* 878(2):116
Price EM, Cleeves LI, Bodewits D, Öberg KI. 2021. *Astrophys. J.* 913(1):9
Price EM, Cleeves LI, Öberg KI. 2020. *Astrophys. J.* 890(2):154
Prinn RG. 1993. In *Protostars and Planets III*, ed. EH Levy, JI Lunine, pp. 1005–28. Tucson: Univ. Ariz. Press
Qi C, D'Alessio P, Öberg KI, et al. 2011. *Astrophys. J.* 740:84
Qi C, Kessler JE, Koerner DW, Sargent AI, Blake GA. 2003. *Astrophys. J.* 597:986–97
Qi C, Öberg KI, Espaillat CC, et al. 2019. *Astrophys. J.* 882(2):160
Qi C, Öberg KI, Wilner DJ, et al. 2013. *Science* 341:630–32
Qi C, Wilner DJ, Aikawa Y, Blake GA, Hogerheijde MR. 2008. *Astrophys. J.* 681:1396–407
Rab C, Elbakyan V, Vorobyov E, et al. 2017. *Astron. Astrophys.* 604:A15
Rab C, Güdel M, Woitke P, et al. 2018. *Astron. Astrophys.* 609:A91
Rab C, Kamp I, Dominik C, et al. 2020. *Astron. Astrophys.* 642:A165
Rivière-Marichalar P, Elliott P, Rebollido I, et al. 2015. *Astron. Astrophys.* 584:A22
Rivière-Marichalar P, Fuente A, Esplugues G, et al. 2022. *Astron. Astrophys.* 665:A61
Ros K, Johansen A. 2013. *Astron. Astrophys.* 552:A137
Rosenfeld KA, Qi C, Andrews SM, et al. 2012. *Astrophys. J.* 757:129
Ruaud M, Gorti U. 2019. *Astrophys. J.* 885(2):146
Salinas VN, Hogerheijde MR, Bergin EA, et al. 2016. *Astron. Astrophys.* 591:A122
Salinas VN, Hogerheijde MR, Mathews GS, et al. 2017. *Astron. Astrophys.* 606:A125
Salyk C, Blake GA, Boogert ACA, Brown JM. 2011a. *Astrophys. J.* 743(2):112
Salyk C, Lacy J, Richter M, et al. 2019. *Astrophys. J.* 874(1):24
Salyk C, Pontoppidan KM, Blake GA, Najita JR, Carr JS. 2011b. *Astrophys. J.* 731(2):130
Sargent AI, Beckwith S. 1987. *Astrophys. J.* 323:294
Schöier FL, van der Tak FFS, van Dishoeck EF, Black JH. 2005. *Astron. Astrophys.* 432:369–79
Schwarz KR, Bergin EA, Cleeves LI, et al. 2018. *Astrophys. J.* 856(1):85
Seifert RA, Cleeves LI, Adams FC, Li ZY. 2021. *Astrophys. J.* 912(2):136
Semenov D, Wiebe D. 2011. *Astrophys. J. Suppl.* 196:25
Semenov D, Wiebe D, Henning T. 2004. *Astron. Astrophys.* 417:93–106

Shu FH, Adams FC, Lizano S. 1987. *Annu. Rev. Astron. Astrophys.* 25:23–81
Siebenmorgen R, Heymann F. 2012. *Astron. Astrophys.* 543:A25
Simon M, Guilloteau S, Beck TL, et al. 2019. *Astrophys. J.* 884(1):42
Smirnov-Pinchukov GV, Molyarova T, Semenov DA, et al. 2022. *Astron. Astrophys.* 666:L8
Smith RL, Pontoppidan KM, Young ED, Morris MR. 2015. *Astrophys. J.* 813(2):120
Stevenson DJ, Lunine JI. 1988. *Icarus* 75:146–55
Sturm JA, McClure MK, Harsono D, et al. 2022. *Astron. Astrophys.* 660:A126
Teague R, Bae J, Bergin EA. 2019. *Nature* 574:378–81
Teague R, Jankovic MR, Haworth TJ, Qi C, Ilee JD. 2020. *Mon. Not. R. Astron. Soc.* 495(1):451–59
Teague R, Loomis R. 2020. *Astrophys. J.* 899(2):157
Teague R, Semenov D, Gorti U, et al. 2017. *Astrophys. J.* 835(2):228
Teague R, Semenov D, Guilloteau S, et al. 2015. *Astron. Astrophys.* 574:A137
Terada H, Tokunaga AT. 2017. *Astrophys. J.* 834(2):115
Terwisscha van Scheltinga J, Hogerheijde MR, Cleeves LI, et al. 2021. *Astrophys. J.* 906(2):111
Thi W, van Zadelhoff G, van Dishoeck EF. 2004. *Astron. Astrophys.* 425:955–72
Thi WF, Hocuk S, Kamp I, et al. 2020. *Astron. Astrophys.* 635:A16
Thi WF, Lesur G, Woitke P, et al. 2019. *Astron. Astrophys.* 632:A44
Thi WF, Mathews G, Ménard F, et al. 2010. *Astron. Astrophys.* 518:L125
Thi WF, Pinte C, Pantin E, et al. 2014. *Astron. Astrophys.* 561:A50
Thi WF, Pontoppidan KM, van Dishoeck EF, Dartois E, d'Hendecourt L. 2002. *Astron. Astrophys.* 394:L27–30
Tielens AGGM. 2008. *Annu. Rev. Astron. Astrophys.* 46:289–337
Tielens AGGM, Hagen W. 1982. *Astron. Astrophys.* 114:245–60
Trapman L, Zhang K, van 't Hoff MLR, Hogerheijde MR, Bergin EA. 2022. *Astrophys. J. Lett.* 926(1):L2
van Boekel R, Min M, Leinert C, et al. 2004. *Nature* 432:479–82
Van Clepper E, Bergner JB, Bosman AD, Bergin E, Ciesla FJ. 2022. *Astrophys. J.* 927(2):206
van den Ancker ME, Bouwman J, Wesselius PR, et al. 2000. *Astron. Astrophys.* 357:325–29
van der Marel N, Booth AS, Leemker M, van Dishoeck EF, Ohashi S. 2021. *Astron. Astrophys.* 651:L5
van der Marel N, van Dishoeck EF, Bruderer S, et al. 2016. *Astron. Astrophys.* 585:A58
van der Marel N, van Dishoeck EF, Bruderer S, Pérez L, Isella A. 2015. *Astron. Astrophys.* 579:A106
van der Marel N, Williams JP, Bruderer S. 2018. *Astrophys. J. Lett.* 867(1):L14
van der Tak FFS, Black JH, Schöier FL, Jansen DJ, van Dishoeck EF. 2007. *Astron. Astrophys.* 468(2):627–35
van der Wiel MHD, Naylor DA, Kamp I, et al. 2014. *Mon. Not. R. Astron. Soc.* 444(4):3911–25
van Dishoeck EF, Bergin EA. 2021. In *ExoFrontiers: Big Questions in Exoplanetary Science*, ed. N Madhusudhan, pp. 14.1–14.15. Bristol, UK: IOP
van Dishoeck EF, Blake GA, Draine BT, Lunine JI. 1993. In *Protostars and Planets III*, ed. EH Levy, JI Lunine, pp. 163–241. Tucson: Univ. Ariz. Press
van Dishoeck EF, Kristensen LE, Mottram JC, et al. 2021. *Astron. Astrophys.* 648:A24
van 't Hoff MLR, Persson MV, Harsono D, et al. 2018a. *Astron. Astrophys.* 613:A29
van 't Hoff MLR, Tobin JJ, Trapman L, et al. 2018b. *Astrophys. J. Lett.* 864(1):L23
van 't Hoff MLR, Walsh C, Kama M, Facchini S, van Dishoeck EF. 2017. *Astron. Astrophys.* 599:A101
van Terwisga SE, van Dishoeck EF, Cazzoletti P, et al. 2019. *Astron. Astrophys.* 623:A150
van Zadelhoff G, Aikawa Y, Hogerheijde MR, van Dishoeck EF. 2003. *Astron. Astrophys.* 397:789–802
Vasyunin AI, Wiebe DS, Birnstiel T, et al. 2011. *Astrophys. J.* 727:76
Visser R, Bruderer S, Cazzoletti P, et al. 2018. *Astron. Astrophys.* 615:A75
Visser R, van Dishoeck EF, Doty SD, Dullemond CP. 2009. *Astron. Astrophys.* 495:881–97
Wakelam V, Herbst E, Loison JC, et al. 2012. *Astrophys. J. Suppl.* 199:21
Wakelam V, Ruaud M, Hersant F, et al. 2016. *Astron. Astrophys.* 594:A35
Walsh C, Millar TJ, Nomura H. 2010. *Astrophys. J.* 722:1607–23
Walsh C, Millar TJ, Nomura H. 2013. *Astrophys. J. Lett.* 766(2):L23
Walsh C, Millar TJ, Nomura H, et al. 2014. *Astron. Astrophys.* 563:A33
Walsh C, Nomura H, van Dishoeck E. 2015. *Astron. Astrophys.* 582:A88
Wei CE, Nomura H, Lee JE, et al. 2019. *Astrophys. J.* 870(2):129

Willacy K. 2007. *Astrophys. J.* 660:441–60
Willacy K, Millar TJ. 1998. *Mon. Not. R. Astron. Soc.* 298:562–68
Willacy K, Woods PM. 2009. *Astrophys. J.* 703:479–99
Williams JP, Best WMJ. 2014. *Astrophys. J.* 788:59
Wilson DJ, Gänsicke BT, Farihi J, Koester D. 2016. *Mon. Not. R. Astron. Soc.* 459(3):3282–86
Woitke P, Kamp I, Antonellini S, et al. 2019. *Publ. Astron. Soc. Pac.* 131:064301
Woitke P, Kamp I, Thi WF. 2009. *Astron. Astrophys.* 501(1):383–406
Woitke P, Min M, Thi WF, et al. 2018. *Astron. Astrophys.* 618:A57
Xu R, Bai XN, Öberg K, Zhang H. 2019. *Astrophys. J.* 872(1):107
Yoshida TC, Nomura H, Furuya K, Tsukagoshi T, Lee S. 2022. *Astrophys. J.* 932(2):126
Young AK, Alexander R, Walsh C, et al. 2021. *Mon. Not. R. Astron. Soc.* 505(4):4821–37
Yu H, Teague R, Bae J, Öberg K. 2021. *Astrophys. J. Lett.* 920(2):L33
Yu M, Evans Neal JI, Dodson-Robinson SE, Willacy K, Turner NJ. 2017. *Astrophys. J.* 850(2):169
Zhang K, Bergin EA, Blake GA, Cleeves LI, Schwarz KR. 2017. *Nat. Astron.* 1:0130
Zhang K, Bergin EA, Schwarz K, Krijt S, Ciesla F. 2019. *Astrophys. J.* 883(1):98
Zhang K, Blake GA, Bergin EA. 2015. *Astrophys. J. Lett.* 806:L7
Zhang K, Booth AS, Law CJ, et al. 2021. *Astrophys. J. Suppl.* 257(1):5
Zhang K, Pontoppidan KM, Salyk C, Blake GA. 2013. *Astrophys. J.* 766:82
Zhang S, Zhu Z, Huang J, et al. 2018. *Astrophys. J.* 869(2):L47
Zhang Y, Snellen IAG, Mollière P. 2021. *Astron. Astrophys.* 656:A76

Contents

Annual Review of Astronomy and Astrophysics
Volume 61, 2023

Indexes

Errata

An online log of corrections to *Annual Review of Astronomy and Astrophysics* articles may be found at http://www.annualreviews.org/errata/astro